# Petrophysics-guided reprocessing of legacyvelocity analysis and seismic data reprocessing to improve mineral exploration targeting in the Irish Zn-Pb Orefield

5 Victoria Susin<sup>1,2</sup>, Aline Melo<sup>1,2</sup>, Koen Torremans<sup>1,2</sup>, Juan Alcalde<sup>3</sup>, David Martí<sup>3</sup>, and Rafael Bartolome<sup>4</sup>

1.2 School of Earth Sciences and Research Ireland Centre for Applied Geosciences (iCRAG), University College Dublin, Belfield, Dublin, Ireland

<sup>3</sup> Geosciences Barcelona GEO3BCN, Barcelona, Spain

<sup>4</sup> Instituto de Ciencias del Mar (ICM) CSIC, Barcelona, Spain

Correspondence to: Victoria Susin (victoria.figueirasusin@ucdconnect.ie)

Abstract. The Limerick Syncline, part of the Irish Zn-Pb Orefield in southwest Ireland, represents a geologically complex and relatively underexplored region, despite hosting several significant mineral deposits, e.g., the Stonepark and Pallas Green, Zn-Pb deposits. The mineralogy and stratigraphic setting of the sulphide mineralisation mineral deposits in the Limerick-Syncline are generally similar to other Irish type deposits. Howeverlargely stratabound Zn-Pb systems hosted within Mississippian carbonates. In the area, a thick volcanic sequence overlies and interfingers with the carbonate host rocks, mineralisation and alteration. This-setting has posed significant challenges to seismic imaging in the region, despite being resulting in a powerful technique for mineral exploration. As a result, the poor understanding of the overall structural setting of the area has remained poorly understood. This study presents an optimised seismic processing workflow tailored to these geological complexities and applied to the legacya 2D seismic reflection profile LK-11-02. The workflow integrates information from newly acquired downhole and laboratory P-wave velocity data with first-arrival travel-time tomography to enhance the accuracy of the produce a new velocity model used for post-stack migration. This resulted in better signal recovery and enhanced reflector coherence, in particular, reflection continuity. As a result, imaging of key stratigraphic boundaries, internal form lines and the lateral interfingering of volcanic and carbonate-volcanic interplay geometries units was enhanced, along with clearer reflection amplitude changes associated with known stratigraphic units. Acoustic impedance analysis using laboratory density data enabled a better understanding of the origins of seismic reflectivity and a more confident geological interpretation of the laterally variable lithologies. The migrated section reveals previously unrecognised major structural features in the Limerick Syncline, enhancing our geological understanding of the region. It highlights the potential of applying this workflow to seismic reflection methods, improving its use as a mineral exploration tool in the Irish Zn-Pb Orefield and similar volcanic-influenced regionsA chaotic, low-amplitude seismic facies was recognised representing laterally persistent breccia corridors which may provide a practical indirect seismic proxy for significantly hydrothermally altered zones in the carbonates. Critically, two major previously unrecognised basin-scale faults were identified to the south of the Stonepark and Pallas Green deposits, bounding a significant (half-)graben. Thickness patterns and igneous packages indicate late Tournaisian to early Viséan syn-depositional faulting coeval with emplacement of the Limerick Igneous Suite, with subsequent Variscan inversion providing a net-zero displacement at the surface. These results expand the exploration research space beyond the known mineralisation areas, especially around normal faults on the southern flank of the Syncline.

#### 1 Introduction

15

20

25

35

The transition to a low-carbon society has significantly increased the demand for essential resources in recent years, driving higher consumption of base metals and critical materials needed for advancing sustainable technologies (Vidal et al., 2013;

Formatted: Not Superscript/ Subscript

Formatted: Superscript

Formatted: Font color: Auto

Formatted: Space After: 6 pt

Ali et al., 2017). Meanwhile, the depth to target across the mining industry continues to increase globally (Alcalde et al., 2022). Specifically in Europe, the recent Critical Raw Materials Act (CRMA) has reinforced the need for sustainable sourcing of critical raw materials within the European Union (Hool et al., 2024), requiring increasingly comprehensive analysis of the subsurface resources. This incentivises the development of cost-effective, more sustainable and high-resolution geophysical methods for mineral exploration (Malehmir et al., 2020; Alcalde et al., 2022).

45

Due to the relatively limited resolving power of traditional mining geophysical methods—a such as electromagnetics, induced—polarisation, and potential field techniques—a at greater depths, the adoption of methods from the oil and gas industry has gradually become more common in mineral exploration (Eaton et al., 2003). The seismic reflection method can provide high-resolution images of the subsurface with a greater penetration depth, complementing and defining target areas for drilling campaigns, which has led to the growing interest in seismic methods as a mineral exploration tool—(Malehmir et al., 2012). Its relatively recent success in imaging and characterising mineral prospects and their structural controls, depth extensions, and host rock properties has been highlighted in multiple studies (e.g., Eaton and Adam, 2010; Malehmir et al., 20122010; Manzi et al., 2019; Malehmir et al., 2020; Gil et al., 2021; Cheraghi et al., 2023; Bell et al., 2023).

In Ireland, 2D seismic surveys have been conducted to better understand the structural and stratigraphic setting of the Irish Mississippian basins to assist exploration for Irish Type\_type Zn-Pb deposits (e.g., de Morton et al., 2015; Ashton et al., 2018). These deposits are hosted within hydrothermally altered carbonate rocks and are predominantly associated with normal faults in relay-ramp systems (Wilkinson and Hitzman, et al., 2015). Spanning an area of approximately 40,000 km², the Irish Orefield has been a significant focus of exploration. Since the 1950s, five deposits, including Lisheen, Galmoy and the world-class Navan deposit, have been developed into producing mines (Blaney and Redmond, 2015).

Ashton et al. (2018) reported the successful application of seismic reflection <u>surveys</u> to the discovery of the Tara Deep deposit at depths of 1,500 meters; in the vicinity of the Navan deposit. Currently, around 1000 line-approximately 1,000 km of 2D reflection seismic exists across the Irish Midlands.

As part of mineral exploration efforts, six 2D seismic reflection profiles were acquired in 2011 near the Stonepark and Pallas Green Zn-Pb deposits, on the northwestern edge of the Limerick Syncline, the study area of this contribution, in southwest Ireland (Fig. 1). The Stonepark deposit has a resource of 5.1 Mt grading 8.7% Zn and 2.6% Pb at depths of 200 meters, and the Pallas Green deposit, a resource of 45.4 Mt grading 7% Zn and 1% Pb at depths between 200 and 1,000 meters (Gordon et al., 2018; Blaney and Coffey, 2023).

In this area, the carbonate rocks that host the sulphide mineralisation are intruded by and interbedded with a thick volcanic succession (Blaney and Coffey, 2023), whose distribution is still poorly understood. Volcanic rocks pose difficulties for seismic imaging because of signal attenuation (Liberty et al., 2015; McBride et al., 2021) and scattering, caused by abrupt vertical changes in elastic properties (e.g., Pujol et al., 1989; Planke et al., 1999; Ziolkowski et al., 2003; Sullivan et al., 2011). These effects have discouraged further seismic exploration in the target area due to the low resolution obtained in previous imaging efforts.

The effectiveness of seismic methods is highly site- and geology-dependent (Malehmir et al., 2012). In geologically complex settings likesuch as the Limerick Syncline, characterised by abrupt lateral facies changes (Somerville et al., 2011), effective seismic processing with suitable velocity models and migration algorithms is crucial to achieve a reliable seismic image (Singh and Malinowski, 2023), Additionally, lithological and petrophysical characteristics of the stratigraphic units, especially the volcanic rocks, must be considered during data processing to ensure accurate imaging and preserve true amplitude responses (Planke et al., 1999). However, suitable velocity modelscharacterisation, and well-constrained petrophysical data are currently

Formatted: Space After: 12 pt

Formatted: Font color: Auto

Formatted: Font color: Auto

missing for the Irish Midlands, especially for the Limerick Syncline. Furthermore, a robust interpretation of the acoustic impedance variations and of the origin of seismic reflectivity remains absent in this part of the basin.

Therefore, to address these data gaps and improve these ismic imaging of the subsurface of the study area, we developed and implemented a reprocessing workflow on the legacy profile LK-11-02 to establish a benchmark for seismic data processing enhance data interpretability, in the Irish Mississippian, applied to the Limerick Syncline area (Fig. 1). This The objective of this work is to improve subsurface characterisation by revisiting mineral exploration seismic datasets and integrating newly acquired information. The new processing sequence incorporates information from recently acquired downhole and laboratory petrophysical data, along with first-arrival travel-time tomography, which provided essential insights into the velocity field, distinguishing it from previous seismic reflection workflows.

We also present an interpretation of the newa velocity data, analysis exploring the petrophysical characteristics of the main units in the Limerick Syncline and how the laboratory P-wave velocity correlates with the travel-time tomography. WeThis analysis was used this information to build a new inform the construction of the stacking velocity model, leading to an improved seismic image with enhanced resolution. Using the resulting improved image, we provide anThe workflow enabled

-	Formatted: Font color: Auto
-	Formatted: Font color: Auto
	Formatted: Font color: Auto
1	Formatted: Font color: Auto
	Formatted: Font color: Auto
()	Formatted: Font color: Auto
	Formatted: Font color: Auto
	Formatted: Font color: Auto
(	Formatted: Font color: Auto
1	Formatted: Font color: Auto

interpretation highlighting of the main lithologic boundaries and fault zones, discussing highlighting the potential of seismic imaging in the subsurface characterisation and its implications for mineral exploration of the area.

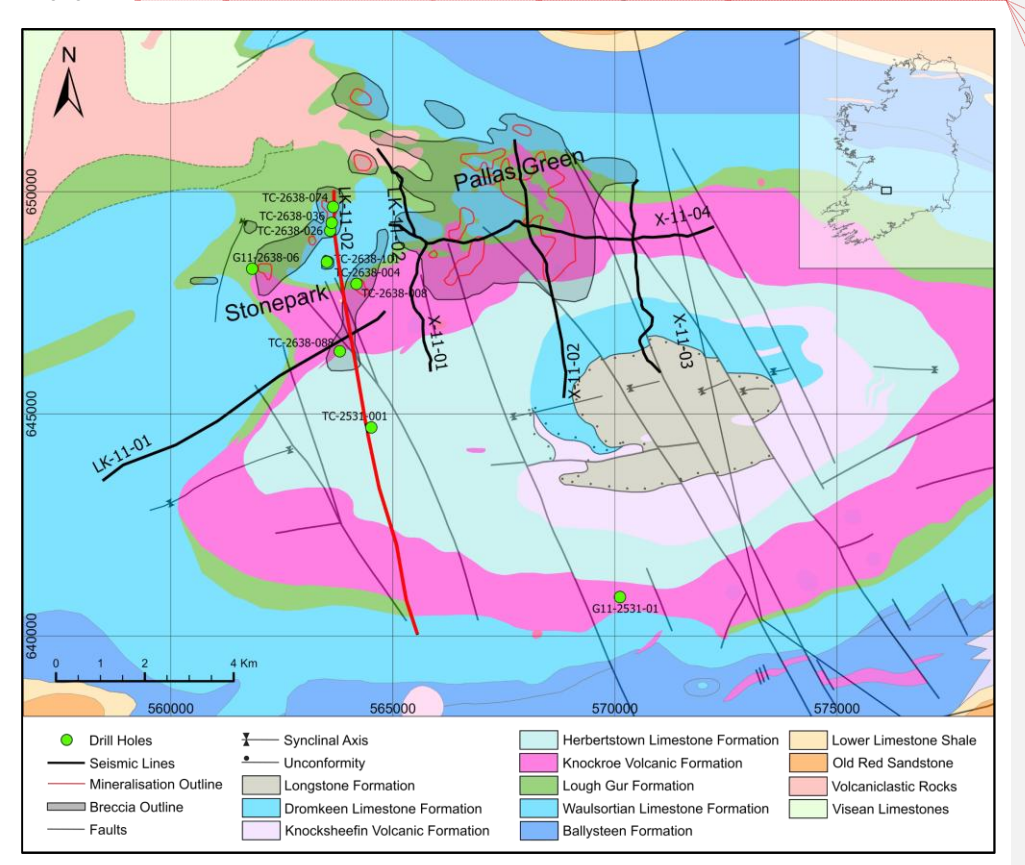


Figure 1: Geological map of the Limerick Syncline 1:100,000 (Geological Survey Ireland, 2022) showing the seismic lines with profile LK-11-02 highlighted in red, the drill holes used for downhole and laboratory petrophysical measurements (green circles) and the location of the Stonepark and Pallas Green prospects. The inset shows the location of part of the Limerick Syncline study area (black rectangle) within Ireland.

#### 2 Geological setting

95

105

The Limerick Syncline hosts a stratigraphic sequence consisting of siliciclastic, carbonate and volcanic rocks (Somerville et al., 1992; Fig. 2). The Lower Palaeozoic basement, underlying the basinal succession, consists of greywackes, shales and volcanic rocks deformed and weakly metamorphosed during the Caledonian orogeny (Chew and Stillman, et al., 2009). Lying unconformably atop the basement are largely Devonian continental red bed conglomerates, sandstones, and mudrocks of the Old Red Sandstone Formation, likely deposited in grabens. A northward-directed marine transgression across Ireland occurred during the early Mississippian, depositing progressively deeper marine carbonates (Sevastopulo and Wyse Jackson, 2009). The oldest transgressive unit is the Lower Limestone Shale Group (LLS), comprising a heterolithic series of interbedded shales, siltstones and sandstones, and carbonates (Somerville and Jones, 1985; Tyler, 1997; Blaney and Redmond, 2015). A transition to fully marine sedimentation followed in an open carbonate ramp environment, consisting of a sequence of argillaceous bioclastic limestones (ABL) of the Ballymartin Formation and Ballysteen Formation, together forming the Ballysteen Group.

Formatted: Font color: Auto

Finally, increasing water depths allowed the development of laterally extensive sequences of micritic mud mounds of the Waulsortian Limestone Formation (WAL; Somerville and Jones, 1985).

Above the WAL lies the Lough Gur Formation (LGG), a cherty, bioclastic, argillaceous limestone, succeeded by the Knockroe Volcanic Formation (KKR), part of the Limerick Igneous Suite and comprising a series of basaltic lavas and pyroclastic strata variably altered and brecciated (Strogen, 1988; Somerville et al., 1992; Blaney and Coffey, 2023); Slezak et al., 2023). The KKR is interfingered with the carbonate beds of the LGG and the overlying Herbertstown Limestone Formation (HBN), dominated by grainstones and packstones of shallow—water origin (Somerville et al., 1992). Towards the top, HBN is interbedded with the Knocksheefin Volcanic Formation (KKS), the second volcanic unit of the Limerick Igneous Suite, consisting of variably altered basanites and tuffs. Chlorite-clay alteration is typically seen in both KKR and KKS (Slezak et al., 2023). The interfingering of volcanics and carbonates forms a package up to 900 meters thick in the Limerick Syncline. These units are cut by later porphyritic basalt dykes and sills (Strogen, 1983; Slezak et al., 2023).

110

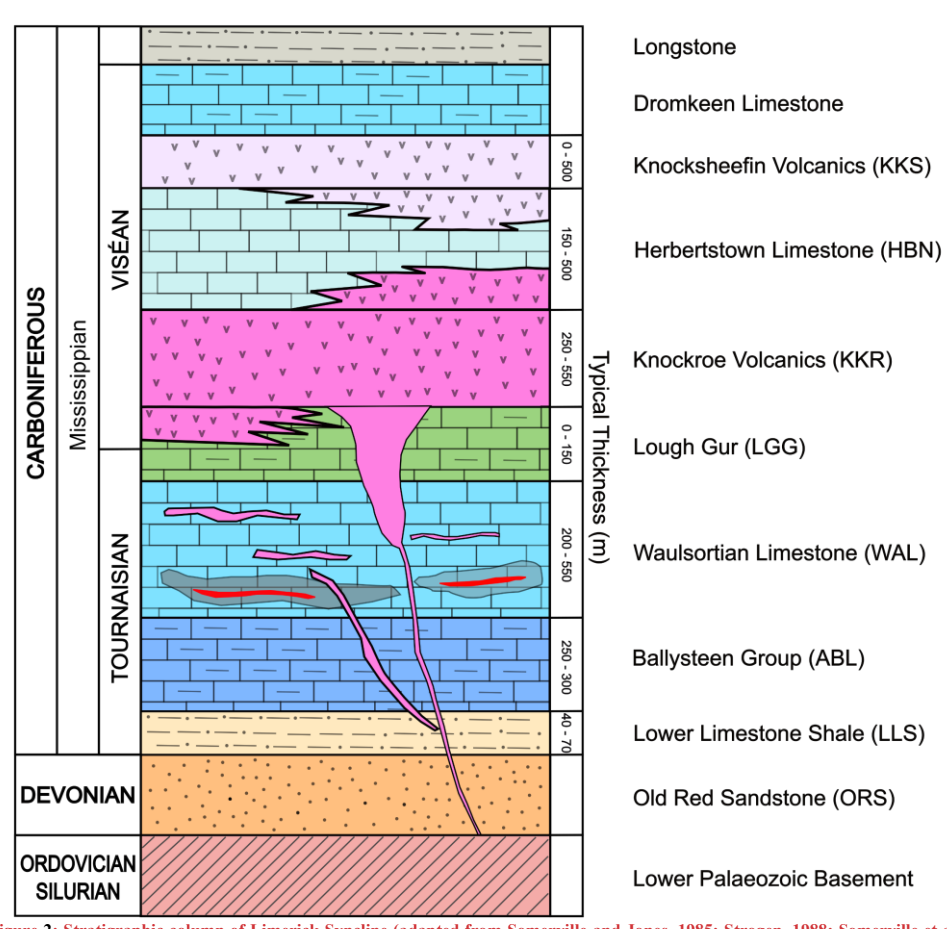


Figure 2: Stratigraphic column of Limerick Syncline (adapted from Somerville and Jones, 1985; Strogen, 1988; Somerville et al., 1992; Blaney and Redmond, 2015). Brecciated zones are drawn in grey, Zn-Pb mineralisation in red and intrusions in pink.

The Waulsortian-hosted Zn-Pb deposits occur largely in the hanging walls of complexly segmented relay-ramp normal fault systems (Hitzman, 1999; Torremans et al., 2018; Kyne et al., 2019). These fault zones are associated with Early Mississippian rifting in the Midlands, having a similar age to the upper ABL and WAL deposition (Johnston et al., 1996; de Morton et al., 2015). Previously, Somerville and Strogen (1992) have argued the absence of syn-sedimentary faulting in the Shannon Trough, and to date, no large ore-controlling faults have been identified in the study area (Blaney and Redmond, 2015). Blaney and Coffey (2023) discuss the association between intrusions in the Limerick Syncline and syn-volcanic faults, and the possibility that these faults were the primary conduits for mineralising fluids. In the study area, most of the mineralisation occurs within the lower half of the WAL as stratiform—lenses hosted by breccia bodies. Brecciation and mineralisation formed through alteration and precipitation-dissolution processes by hydrothermal fluids (Blaney and Redmond, 2015).

3 Data and Methods

120

125

30

35

This study focuses on the petrophysics-guided velocity analysis and the seismic reprocessing of profile LK-11-02, which is part of a series of 2D surveys acquired on the northwestern edge of the Limerick Syncline (Fig. 1). Figure 3 illustrates the The workflow employed in this study. The processing workflow incorporates new acquisition(Fig. 3) consists of (i) combining newly acquired on-core petrophysical data through laboratory measurements and the use of legacy, downhole sonic log data. This data was used to produce an iteratively refined velocity analysis, integrating P-wave velocity (Vp) from the laboratorydata, and downhole petrophysics, travel-time tomography from legacy first break picks, and to produce a velocity analysis that constrains the velocity field of the area, (ii) using this velocity information to guide semblance analysis from legacy CDP gathers. Two legacy seismic for stacking velocity construction, and (iii) reprocessing profile LK-11-02, originally

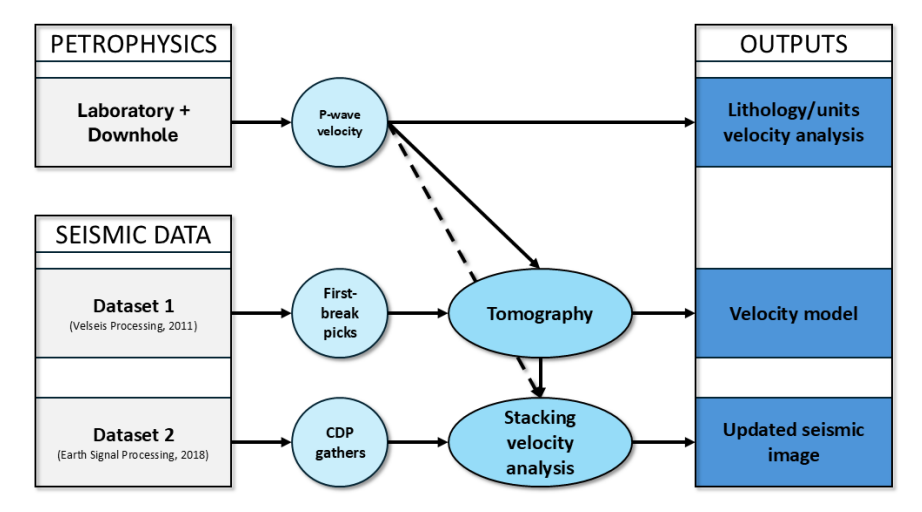


Figure 3: Flowchart showing the data and processing workflow used in the study. Dataset 1 and dataset 2 comprise the data made available for the reprocessing. Outputs are the workflow and products developed to improve the seismic image.

processed in 2011 and reprocessed in 2018 (here referred to as datasets were used as input for 1 and 2, respectively), by incorporating the 2018 products together with the new processing, which included an optimised velocity analysis and time migration-updated velocity model. Additionally, acoustic impedance data werewas derived from the petrophysical properties to assist in provide further constraints for a more comprehensive-and, geology-driven seismic interpretation- of the new seismic image.

Formatted: Font color: Black

Formatted: Font: 10 pt

#### 140 3.1 Drill hole data

45

150

155

Ten drill holes with associated geological logs were made available for studied in detail as part of this work. Drilled, with drilled depths rangeranging from 350 to 900 meters (Table 1; Fig. 4). Eight of thesethe drill holes, including TC-2531-001 (Chakraborti et al., 2025), TC-2638-004 (Susin et al., 2025b), TC-2638-008 (Susin et al., 2025c), TC-2638-026 (Susin et al., 2025d), TC-2638-036 (Susin et al., 2025e), TC-2638-074 (Susin et al., 2025f), TC-2638-088 (Susin et al., 2025g), and TC-2638-101 (Susin et al., 2025h), are located on or near the seismic profile trace, while the The remaining two (, G11-2531-01 (Melo et al., 2025a) and G11-2638-06) (Susin et al., 2025a), are situated 4.9 and 1.8 km away, respectively (Fig. Table 1). The Most drill holes predominantly intersect the thick accumulations of WAL, and typically finishing severalterminate a few meters into the underlying ABL. Only two Six of the eighten drill holes along the seismic line sample the shallower also intersect higher stratigraphic units.-, including the LGG, KKR, HBN, and KKS (Fig. 4).

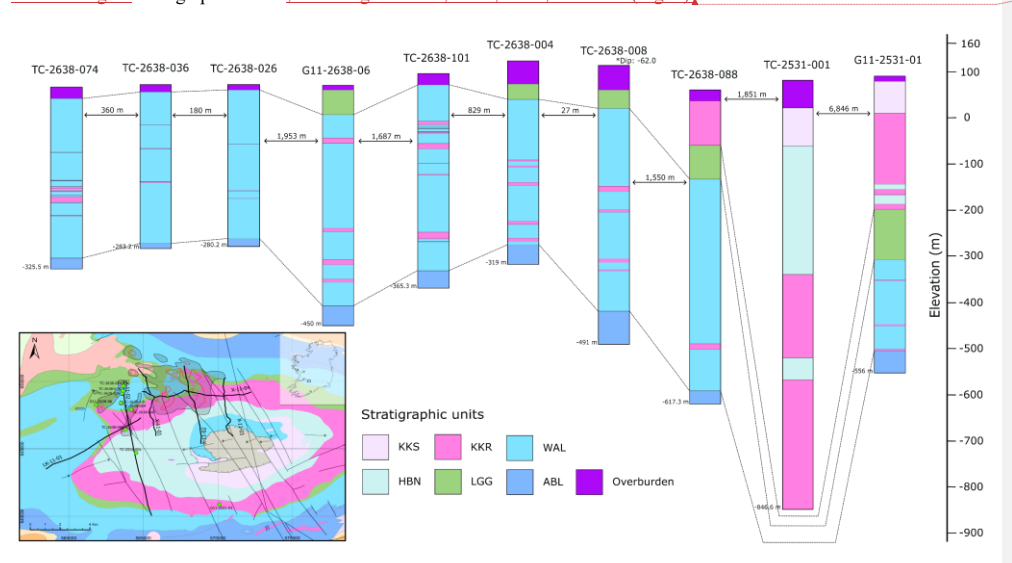


Figure 4: Lithological sections relative to the topography and distance between drill holes. Stratigraphic information is derived from geological logs.

The top of drill hole TC-2638-088 (Fig. 44) intersects the KKR for 95 meters, followed by 70 meters of LGG before reaching the WAL and the top of the ABL. South of TC-2638-088, in the central part of the seismic profile, the drill hole TC-2531-001 is the deepest in the region, providing 926.60 meters of stratigraphic information in the central part of the Limerick Syncline. It crosses a thick—interfingering, interfingered carbonate-volcanic sequence, intersecting the KKS, transitioning to the carbonates of the HBN, and exhibiting predominantly lavas and tuffs from 420 meters depth until the bottom.

**Table 1** Drill hole information for petrophysical measurements with the formations intersected and the and distance to the seismic profile LK-11-02.

DRILL	DEDTIH	TOTAL	DICTANCE TOP	INTERSECTED
HOLE Drill	DEPTHLengt	SAMPLES Total	DISTANCE TO Distance	<b>FORMATIONS</b>
Hole ID.	<u>h</u> (m)	Samples	<u>to</u> LK-11-02	
HOIC ID,		Samples		
TC-2531-001	926.6	199	144 m	KKS, HBN and KKR

Formatted: Font color: Red

Poleted Cells
Formatted: Line spacing: 1.5 lines
Formatted: Font: Bold
Formatted: Font: Bold
Formatted: Font: Bold
Formatted: Font: Bold
Formatted: Line spacing: 1.5 lines

				WAL and ABL		
TC-2638-004	440	50	430 m		•	Formatted: Line spacing: 1.5 lines
						Formatted Table
TC-2638-008	605	51	430 m	WAL and ABL	-	Formatted: Line spacing: 1.5 lines
TC-2638-026	349.6	50	120 m	WAL and ABL	•	Formatted: Line spacing: 1.5 lines
TC-2638-036	352.5	39	78 m	WAL and ABL	4	Formatted: Line spacing: 1.5 lines
TC-2638-074	389.5	50	20 m	WAL and ABL	-	Formatted: Line spacing: 1.5 lines
TC-2638-088	677.3	50	297 m	LGG, WAL and ABL	•	Formatted: Line spacing: 1.5 lines
TC-2638-101	461.3	50	195 m	WAL and ABL	4	Formatted: Line spacing: 1.5 lines
G11-2531-01	520	84	4,890 m	KKS, HBN, KKR, LGG and WAL	-	Formatted: Line spacing: 1.5 lines
G11-2638-06	518.6	88	1,830 m	LGG, WAL and ABL	4	Formatted: Line spacing: 1.5 lines

Drill holes G11-2531-01 and G11-2638-06 (Fig. 14), located a few kilometres away from the seismic profile, provide important downhole petrophysical information about the stratigraphic sequence of the north and south flanks of the Syncline. Both drill holes cross the stratigraphy from the LGG to the ABL. G11-2531-01 intersects approximately 300 meters of interfingered volcanic and carbonate rocks before reaching the LGG.

## 3.2 Petrophysics data

160

165

170

175

Laboratory P-wave velocity (Vp) and density data were acquired for over 700 core samples, covering the full length of the available drill holes. Measurements were conducted on NQ-sized samples, each 10 centimetres in length. The sampling interval was planned based on the total drill hole length, aiming for approximately 50 samples per drill hole, except for TC-2531-001, G11-2531-01 and G11-2638-06, where denser sampling was carried out (Table 1). In addition to the laboratory measurements, drill holes G11-2531-01 and G11-2638-06 (Fig. 1) include legacy downhole sonic log datadatasets.

The Vp measurements were taken on dry core samples using a Proceq Pundit Lab ultrasonic pulse velocity device; (Melo et al., 2025b). Grain size variations in the samples can influence the pulse propagation. This effect can be minimised by selecting a frequency such that the wavelength is at least twice the size of the largest grains (Proceq Pundit Lab manual). In our study, the samples consist primarily of volcanic and carbonate rocks from the KKR, WAL and ABL (Fig. 24). A frequency of 150 kHz was selected, assuming a wavelength twice as large as the coarsest particles in the samples, such as fossils. Quality control was applied to the dataset, including filtering to retain only measurements with an accuracy greater than 75%.

The density measurements were taken on the same core samples, which were soaked in water for 24 hours before measurement, using an Ohaus Explorer balance equipped with an under-hook weighing system. (Melo et al., 2025b). Density iswas calculated using the Archimedes principle, which consists of weighing the sample in both air and water. The water temperature iswas considered in the calculation.

The legacy sonic log data from the two drill holes was acquired using full-waveform sonic probes. These probes employ dual transmitters and receivers to emit and detect high-frequency acoustic waves, measuring the first-arrival transit time of P-waves

85

90

200

205

210

through the formation. The precise distance between the transmitters and receivers enables computation of the formation acoustic velocity (Robertson Geo Mining & Minerals, 2019).

#### 3.3 Travel-time tomography

The To extend the velocity analysis beyond 1D velocity measurements from drill holes, a tomographic velocity model was obtained from profile LK-11-02, using the PStomo\_eq 3D local earthquake (LE) tomography algorithm (Benz et al, 1996; Tryggvason et al., 2002) that also handles the inversion of controlled source data (together and separately). The model is based on the legacy first arrivals-arrival picks from dataset Lused for statics corrections, which were complemented with new travel time pickstimes manually picked at an interval of 250 meters in CMP gathers for far offsets in this study. Forward modelling was performed by computing the time field from a source or receiver to all the model cells-, sized 40 m x 10 m x 5 m (for x, y, z). Then, the travel times to source and receiver positions were calculated from the time field and the ray tracing was performed backwards and perpendicular to the isochrons (Tryggvason and Bergman, 2006). The inversion part of the processing is performed with the conjugate gradient solver LSQR (Least Squares QR; Paige and Saunders, 1982).

An appropriate initial velocity model is essential to ensure convergence during travel-time inversion. A smooth 2D model was developed in this study, utilising a priori constraints from the petrophysical Vp data and drilling control on formation depths in the area. The model was generated from a set of 1D velocity profiles, incorporating shallow velocity estimates and a gradual increase in velocity with depth, using values extracted from the petrophysical dataset. The simplicity of the model was supported by the robustness of the inversion algorithm, which enabled effective use of these generalised velocity trends. Equally important is the accurate picking of first arrivals, which serve as the primary constraint for the tomographic inversion. Therefore, careful quality control and validation of the first-arrival times, including both legacy and new picks, were crucial to ensure the effective performance of the tomographic inversion. Inaccurate or inconsistent picks can lead to significant errors in the velocity model, potentially hindering convergence and reducing the reliability of the results.

## 3.4 Seismic imaging

### 3.4.1 Legacy seismic Seismic data available

The available legacy data of the 10.9 km long lineProfile LK-11-02 wasconsists of a 10.88 km line acquired using a split-spread geometry with a Vibroseis seismic source, featuring a 20-meter m source spacing and a 10-meter m receiver spacing.

The seismic data available. The sweep ranged from 8 to 160 Hz over 16 s with a taper of 300 ms. Data was recorded with a 1 ms sampling interval and a total record length of 3000 ms. Near and far offsets are 5 m and 2995 m, respectively.

The data available in the study consists of two datasets (Fig. 3): i) the raw

- i. Dataset 1: Raw field data, and the processed stack, and post-stack time migration delivered to Teck Resources Limited by Velseis Processing Ltd. and available at the in 2011, licensed from the Geoscience Regulation Office Department of Climate, Environment, and Communications of the Government of Ireland Exploration and Mining Division, referred to in the section as legacy dataset 1; and ii) CDP.
- <u>ii.</u> <u>Dataset 2: CMP</u> gathers (containing geometry, statics correction, and de-noising), stack, and pre-stack time migration, processed by Earth Signal Processing Ltd. (ESP) and availablein 2018 for this study through Group Eleven Resources, which is referred to as legacy dataset 2. This study uses these used under license.

Formatted: Font color: Auto

Formatted: Font color: Auto
Formatted: Font color: Auto
Formatted: Font color: Auto
Formatted: Font color: Auto
Formatted: Font color: Auto
Formatted: Font color: Auto

Formatted: Font color: Auto
Formatted: Font color: Auto
Formatted: Font color: Auto
Formatted: Font color: Auto
Formatted: Font color: Auto

Formatted: Font color: Auto

These two legacy datasets serve as starting points for the new processingour workflow. First-arrival picks extracted from the header of dataset 1 were quality-checked, corrected and complemented for tomographic inversion. CMP gathers from dataset 2 were used to generate the new seismic image.

While standard seismic pre-processing techniques were applied, this study does not focus on their evaluation. Instead, it emphasises the impact of incorporating additional information inteabout the velocity field, refining the velocity model and improving post-stack processing.

The historic processing workflowsworkflow for the legacy datasets 1 and dataset 2 areis described in Table 2. Dataset 2 differs slightly from dataset 1 by applying a differentIt applies a pre-processing sequence to enhance the signal-to-noise (S/N) ratio in the raw data. In dataset 2, ESP reports the application of, a surface-consistent amplitude scaling to address variable source and receiver coupling, and residual scaling to enhance offset contribution and to preserve amplitudes in noisy areas. A different set of statics corrections was also applied by ESP, minimising travel-time distortions in the CMP gathers and improving the stack response. Other significant differences include the post-stack processing and the The Kirchhoff pre-stack time migration, which was applied using 100% of the smoothed stacking velocities. The dataset 2 pre-processed CDP gathers (Table 2) are the input dataset for our new processing.

Table 2 Processing workflows of the legacy datasets available for the study. In this study, we use the first break picks from dataset 1 and the CDP gathers (containing geometry, statics correction, and de-noising) from dataset 2.

#### Table 2 Processing workflow of dataset 2.

220

225

230

	Geometry and QCTrace	1.12. Surface consistent statics Geometry and OC
2.	aditing	
2.	<del>curing</del>	Juliace consistent station
	Geometry Refraction	2.13. Refraction Final semblance velocity analysis:
	analysis	Picks 250 m interval
3.	Static	
	computationReplacement statics:	3-14. Coherent noise attenuation: 12 Hz cut-offReplacement
	Datum: 2000 m, replacement velocity 45003500 m/s	statics: Datum: 0 m, replacement velocity 3500 m/s
	Trace editing Amplitude	15. Spectrum analysis (shots)Trace editing
	recovery	4- <u>16. Mute</u>
	Exponential scalingFan filter, linear noise: 6-30 Hz	5-17. Sort to CMP gathers Exponential scaling
6.	Amplitude	6.18. Migration
	scaling Deconvolution:	Kirchhoff pre-STM using 100% of smoothed
	100ms operator	velocityAmplitude scaling
7.	Vibroseis	
	designature Velocity analysis 1: Picks 500 m interval	7.19. Spectrum analysis (gathers)Vibroseis designature
8.	Fourier filter:	
	0-1000 m/s velocity, 0-28 Hz frequencyStatic calculation and application	8.20. Final muteFourier filter: 0-1000 m/s velocity, 0-28 Hz frequency
9.	Deconvolution: 5/8 – 130/150 HzVelocity	9-21. Stack Deconvolution: 5/8 – 130/150 Hz

Deleted Cells	
Formatted: Font: Bold, Font color: Auto	
Formatted Table	
Formatted: Font color: Auto	)
Formatted	
Formatted: Bullets and Numbering	(
Formatted	
Formatted	
Formatted: Bullets and Numbering	
Formatted	
Formatted	
Formatted	
Formatted: Bullets and Numbering	
Formatted	
Formatted: Bullets and Numbering	
Formatted	
Formatted	
Formatted	
Formatted: Bullets and Numbering	
Formatted	
Formatted	
Formatted	
Formatted: Bullets and Numbering	
Formatted	
Formatted	
Formatted	()
Formatted: Bullets and Numbering	(
Formatted	
Formatted	
Formatted	
Formatted: Bullets and Numbering	
Formatted	
Formatted	
Formatted	
Formatted	
Formatted: Pullate and Numbering	<u> </u>

Formatted: Bullets and Numbering

analysis 2: Picks 250 m interval 10. Static calculation and application 2Residual Residual Multichannel trace, scaling scaling. 112. Velocity analysis 1: 11. AGC: 300 ms Picks 500 m interval 12. DMO: 122. Surface consistent statics Velocity of 4000 m/s <u>VelocitySemblance velocity</u> analysis <u>Filter: 25/40 – 65/75 Hz</u>Final on DMO gathers1: velocity analysis: Picks 500 m interval Picks 250 m interval 14. NMO: 142. Coherent noise attenuation: 12 Hz cut-off 30% stretch mute 15. Stack 152. Spectrum analysis (shots) 16. Migration: 162 Sort to CMP gathers Phase shift using 100% of smoothed velocity 172. Migration 17. Band-pass filter: 40-18 140-72 Hz-dB Kirchhoff pre-STM using 100% of smoothed velocity 18. AGC: 300 ms 182. Spectrum analysis (gathers) 192. Final mute 202.Stack 212. Multichannel trace scaling 222.Filter: 25/40 - 65/75 Hz

3.4.2 New seismic data processing

It is important to note that full recovery of the original seismic products was not possible. Using two datasets reflects a common challenge in mining, imposing practical limitations on legacy data availability, including incomplete records, missing processing parameters, and limited documentation of prior workflows.

#### 3.4.2 Reprocessing workflow

235

240

245

Our seismic processing workflow is outlined in Table 3. It focused on improving the producing a velocity analysis infor the area and incorporating the new information into the seismic processing applied in our study.

The new workflow workflow uses CMP gathers from step 17 in Table 2 as input and includes semblance velocity picking, normal moveout correction (NMO), CDPCMP stacking, de-noising, and post-stack time migration. Our The stacking velocity model is guidedinformed by petrophysicspetrophysical and tomographic results following the normal moveout correction. In qualitative terms, when both laboratory Vp and tomography indicate high velocities in the shallow carbonate units, the stacking velocity is adjusted to reflect these values, aligning both the geological setting and the need to flatten reflectors during the velocity analysis.

The velocities were picked at an interval of 250 m based on the interactive normal-moveout correction and guided by the average velocity model obtained from the tomographic inversion and petrophysical measurements. After quality control of the stack section, we applied an additional de-noising sequence including Butterworth filtering, time-frequency domain (TFD) noise attenuation and 2D spatial filtering to suppress remaining coherent and random noise. The <code>lastfinal</code> step in the processing Formatted: Font color: Auto

Formatted: Font color: Auto

Formatted: List Paragraph, Outline numbered + Level: 1 + Numbering Style: 1, 2, 3, ... + Start at: 12 + Alignment: Left + Aligned at: 0.63 cm + Indent at: 1.27

Formatted: Bullets and Numbering

Formatted: Font color: Auto

Formatted: Font color: Auto

Formatted: List Paragraph, Outline numbered + Level: 1 + Numbering Style: 1, 2, 3, ... + Start at: 12 + Alignment: Left + Aligned at: 0.63 cm + Indent at: 1.27

**Formatted Table** 

Formatted: Bullets and Numbering

Formatted: Font color: Auto

Formatted: Font color: Auto

Formatted: Font color: Auto

255

sequence was a Kirchhoff post-stack time migration, intendedusing 100% of the smoothed stacking velocity. Intended to relocate dipping events to their correct positions, collapse diffractions, and increase resolution.

Given the complex geology of the study area and the <u>moderatenoisy</u> data <u>quality</u>, we avoided adding unnecessary complexity to the velocity model. This decision was made to prevent potential challenges and instability in the Kirchhoff time migration, particularly when dealing with sharp velocity contrasts (Pu et al., 2021). For the same reasons, we opted for post-stack migration, as pre-stack migration would require a more detailed velocity model than the data or geology allows.

Table 3 Reprocessing workflow applied to the legacy dataset 2 pre-processed shot CMP gathers.

New	Processing Reprocessing workflow.
1.	Semblance velocity analysis
	Picks 250 m interval
2.	NMO
	30 % stretch mute
3.	Stack
4.	Butterworth filter: 12/17 - 50/100 Hz
5.	FTD noise attenuation
	100 ms window, 5-70 Hz frequency
6.	2D spatial filtering
7.	Migration
	Kirchhoff post-STM using 100% of the
	smoothed velocity

Formatted: Font color: Auto

Formatted: Font color: Auto

Formatted: Font color: Auto

Formatted: Font: Bold, Font color: Auto

Formatted Table

Formatted: Font color: Auto

#### 4 Results

260

265

270

## 4.1 Velocity analysis

P-wave velocities were first measured on the core samples from drill holes G11-2531-01 and G11-2638-06, which were then and compared with the downhole sonic logs to analyseassess the correlation between the values obtained from both two methods. To address the difference indifferent sampling rates between the datasets (i.e. every intervals (1 cm in the sonic logs vs every 10 m on average in the core samples), we resampled the sonic log curve was resampled to a coarser resolution, keeping values anchored at depths corresponding to laboratory measurements (Fig. 5). 4). The methods Both datasets displayed similar Vp trends for Vp, although the sonic logs showedyield slightly higher velocities than the laboratory measurements. The discrepancies. These offsets are likely due attributed to differences in the sampling measurement conditions (e.g. lithostatic vs. atmospheric pressure—), sample state (fresh rock vs-\_time-degraded by time-core samples), pore fluid effects (laboratory measurements were done on dried samples), and equipment frequencies anisotropy, and instrument frequency responses. Nevertheless, the good correlation between the two datasets provided the confidence to extend our sampling velocity analysis campaign to the remaining eight drill holes and acquire velocity information from various locations along the seismic profile, an important step given that downhole petrophysical data is rarely available in mineral exploration. The Vp measurements were used in this study as qualitative geological constraints, validating velocity trends, identifying key velocity contrasts, and informing the velocity picking in ambiguous zones with low semblance coherence.

Formatted: Font color: Auto

Formatted: Font color: Auto

The laboratory Vp dataset, comprising a total of 640 measurements, was eategorised according to the main-classified by stratigraphic units as well as the main lithologies and textural characteristics (Fig. 5). Variations (Table 4). Because velocity in velocity within carbonate rocks are closely related is sensitive to porosity and pore types, with frame-forming pores generally associated with higher velocitiestype (Eberli et al., 2003). Accordingly, the carbonate samples were classified as mudstone, wackestone, packstone, or grainstone. Samples with significantly increased clay content or the presence of chert were classified as argillaceous and cherty, respectively. In addition, features), samples were also visually grouped by lithological and textural characteristics. The main lithological categories are clean (packstones and grainstones), bioclastic (limestones with fossil fragments, typically wackestones) and mud-rich (samples dominated by fine fractions, either micrite or clay/argillaceous). Additional textures, such as dolomitization, brecciation and mineralisation, were also included in the textural classification. Dyke and volcanic samples were also differentiated. However, their textures are not examined in detail in this study.

275

280

285

290

The Vp values of the units in the Limerick Syncline range from 3000 to 6500 m/s. The samples of the KKS identified as dykes and lithic tuffs show a wide range of P-wave velocities (from 3000 to 6000 m/s with a median around 4800 m/s). Intense clay alteration, possibly due to weathering, is a common characteristic amongst the KKS samples and is responsible for decreasing Vp to velocities close to 3000 m/s. The velocity for the KKR ranges from 4600 m/s to 6300 m/s (median of 5600 m/s), and the outliers displaying low velocities correspond mostly to volcaniclastic or tuff samples. The KKR also shows large variations in velocity due to its highly variable package of volcanic rocks, containing lava flows, tuffs and carbonate-rich pyroclastic flows, as per drill core observations.

3100 to 6500 m/s (Table 4). Overall, the velocity contrasts within the stratigraphy are very mild. Notable velocity contrasts are seen at the contact between the volcanic-dominated (KKR and KKS) and the carbonate-dominated (LGG and WAL) units,

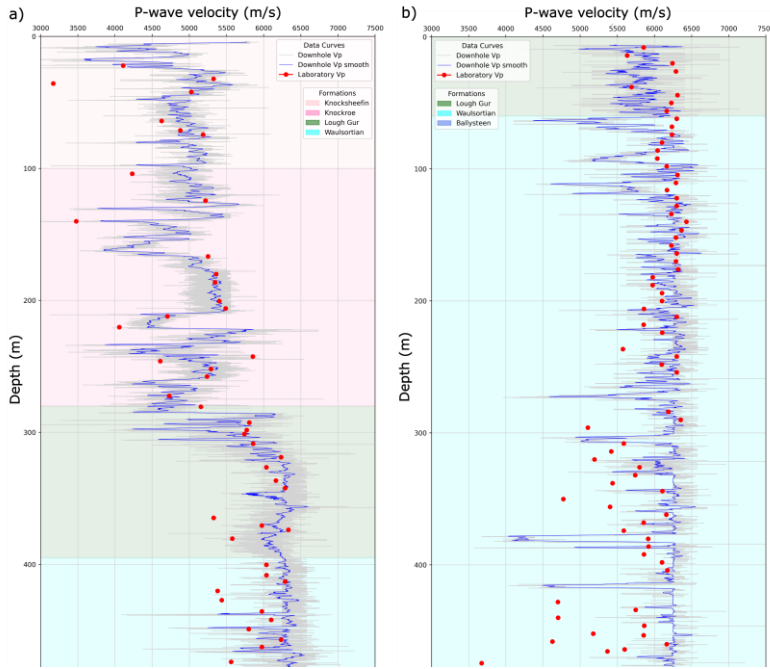


Figure 4: Comparison of downhole and laboratory P-wave velocity data a) for drill hole G11-2531-01, and b) for drill hole G11-2638-06. The light grey curve represents the downhole data, the blue curve represents the resampled downhole data, and the red dots represent the laboratory data. The background colours represent stratigraphic units intersected by the drill holes.

as well as between WAL and ABL (Fig. 5 and Table 4). The carbonate units show higher overall velocities compared to the volcanic rocks. Velocity outliers observed in the carbonate sequence ean beare related to increased elaymud content, dolomitization, brecciation and mineralisation, individually (as individual textures or combined.). The packstones and coral-rich intervals of the HBN show higher velocities with a median value of 6100 m/s, while intervals dominated by wackestones display lower velocities and a median value of 5900 m/s (Fig. 5b). Outliersper texture are not examined in detail in this unit represent volcanic layers interbedded in the HBN limestone sequencestudy.

295

\$00

305

310

315

The LGG is composed of three different facies (Strogen, 1988) that can be identified throughout the samples: a bioclastic chert-rich wackestone, a poorly sorted crinoidal grainstone with rare chert and a non-argillaceous, well-washed grainstone. The higher velocities in the unit (6000 m/s) relate to the samples of non-argillaceous grainstone and chert-rich wackestone. In comparison, low velocities (5800 m/s) are associated with core samples with increased clay content.

The samples of the WAL show a wide range of velocities (Fig. 5). The unit comprises stacked microbial mud mounds with two main facies (Lees et al., 1995). One facies, representing the mud mound core, contains massive mudstones often with stromatactis cavities typically infilled with calcite. The other facies represent flanks of the mud mounds, which are composed of interbedded bioclastic wackestones, packstones and grainstones with variable amounts of wispy argillaceous material. The WAL is also frequently affected by post-depositional processes: it is the main host to Zn-Pb mineralisation and locally shows strong but chaotic dolomitization and brecciation textures, which are all commonly found in the samples. For this unit, velocities range from 3700 to 6500 m/s with a median around 6000 m/s, where increased clay content, dolomitization, and brecciation are common characteristics observed in the low spectrum of the velocity range. Higher velocities (around 6200 m/s) are predominant in the mud mound core facies samples. Intensely dolomitized samples exhibit lower average velocities (around 6000 m/s) with outliers well below 5000 m/s. Dolomitized samples show a wide range of velocities (3700 to 6500 m/s; Fig. 5b), likely reflecting the presence of various types and generations of dolomite. This reflects the observations of Blaney and Redmond (2015), who describe three textural types of dolomites in the WAL in the study area. Breeciated and mineralised samples show velocities ranging from 4700 to 6400 m/s, with a median value of 5800 m/s, and from 5500 to 6400 m/s, with a median of 6100 m/s, respectively. The decrease in velocity relative to the surrounding host rocks caused by these processes appears to depend on the hydrothermal alteration intensity. Intensely brecciated samples show lower velocities than weakly brecciated ones. The high median value in mineralised samples is attributed to the more common presence of pyrite, Formatted: Font: 10 pt

which exhibits higher velocities than sphalerite and galena. This analysis is also reported by Salisbury et al. (2000). Mineralisation and the WAL mudstone show similar velocities (Fig. 5b).

320

325

330

The ABL samples display the lowest velocities of the carbonate sequence, ranging from 5000 to 5800 m/s, with a median of 5700 m/s. This is consistent with the argillaceous bioclastic content of the limestones, with overall clay content representing approximately 30% of the lithology (Sleeman and Pracht, 1999). Clay rich samples reveal velocities between 5000 and 6100 m/s and a median value of 5800 m/s (Fig. 5b).

Overall, the velocity contrasts within the stratigraphic units of the Limerick Syncline are very mild. Notable velocity contrasts can be seen in the contact between the volcanic dominated (KKR and KKS) and the carbonate dominated (LGG and WAL) units, and between the WAL and the ABL (Figs. 4 and 5).

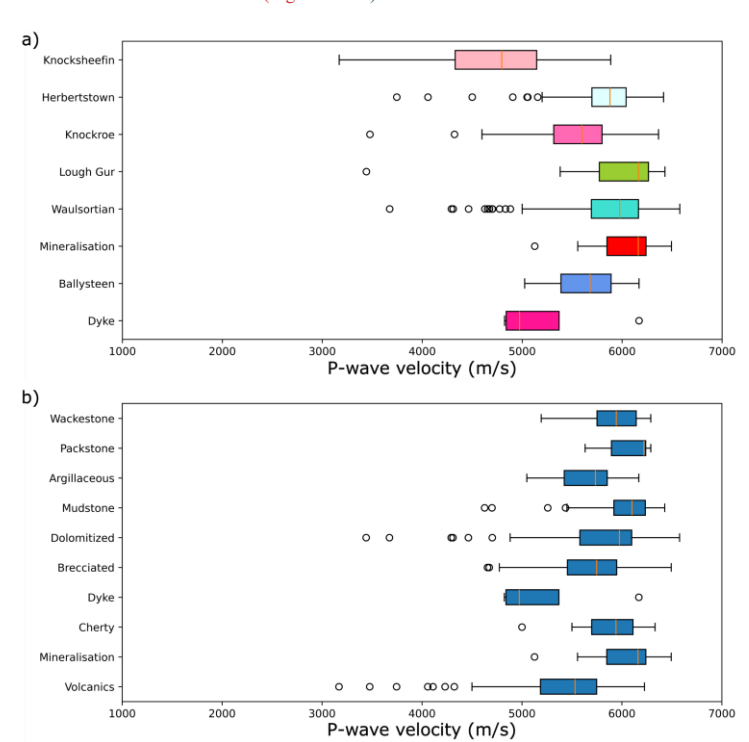


Figure 5: Box plot of the laboratory P-wave velocity data. Median values are represented by the orange line, box length and whiskers vary according to the interquartile range. Outliers are represented by circles. a) Data classified according to the main stratigraphic units in the Limerick Syncline, and b) data classified according to lithology.

To extend and validate the Vp petrophysical measurements over the entire study area, we performed travel-time tomography by inverting first arrival picks from legacy dataset 1, resulting in a P-wave velocity model (Fig. 6). The velocity field was resolved upfrom the surface topography down to a maximum depth of 245 m. The resolution in travel-time tomography is strongly constrained by the available offsets and the seismic velocities involved in the inversion, which determines the final ray coverage used to plot the velocity models. For this reason, new picks for far offsets were included in the inversion, although these were limited because of the low S/N ratio in some of the acquired seismic reflection data.

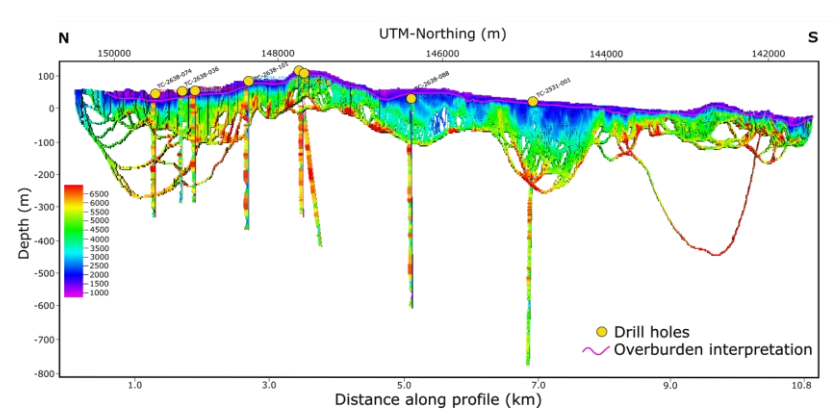


Figure 6: Travel-time tomography model displaying P-wave velocity data alongside petrophysical velocity measurements from the drill hole samples (marked by the yellow circles). The purple line outlines the overburden thickness interpreted from the model and drill hole data.

<b>Units</b>	Velocity (m/s)	Median (m/s)	Lithology/Texture	Velocity (m/s)	Median (m/s)
KKS	3100 - 5900	<u>4800</u>	<u>Clean</u>	<u>5800 – 6400</u>	<u>6100</u>
<b>HBN</b>	5300 - 6400	<u>5900</u>	<b>Bioclastic</b>	5600 - 6300	<u>6000</u>
KKR	3500 - 6300	<u>5600</u>	Mud-rich	5000 - 6200	<u>5700</u>
<b>LGG</b>	5400 - 6400	<u>6100</u>	<b>Dolomitized</b>	3700 - 6400	<u>6000</u>
WAL	3700 - 6500	<u>6000</u>	<b>Brecciated</b>	4600 - 6500	<u>5700</u>
ABL	5000 - 6200	<u>5700</u>	Mineralised	5100 - 6500	<u>6200</u>

The uppermost layer in the model, <u>outlined by a purple line in Fig. 6</u>, shows a low-velocity zone (purple to blue colours, ≤ 2000 m/s) with a thickness ranging from 10 to 50 m, which, <u>according to core logging data</u>, can be correlated with the overburden-in the area according to core logging data. Below the immediate overburden, a thick low-velocity zone (≤ 3500 m/s) appears in the centre of the profile, south of 146000mN, thickening up to 170 meters close to drill hole TC-2638-088, <u>(arrows 1 and 2)</u>, and reducing in thickness around 144000mN. These lower velocities correspond to altered volcanic rocks from the KKS and KKR units in TC-2531-001 (0 to -60 m-MSL) and TC-2638-088 (30 to -60 m-MSL). Laboratory measurements for these intervals also reveal relatively reduced velocities between 4700 and 5900 m/s and 4800 and 5400 m/s,

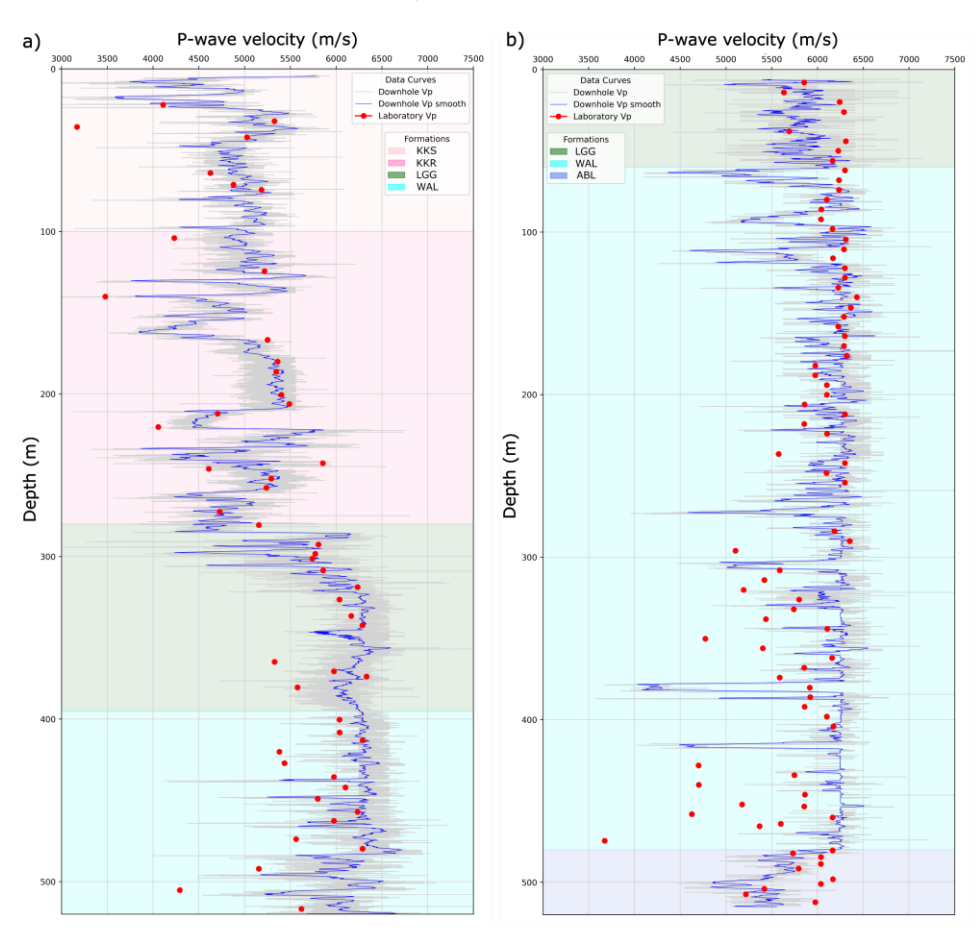


Figure 5: Comparison of downhole and laboratory P-wave velocity data a) for drill hole G11-2531-01, and b) for drill hole G11-2638-06. The light grey curve represents the downhole data, the blue curve represents the resampled downhole data, and the red dots represent the laboratory data. The background colours represent stratigraphic units intersected by the drill holes.

respectively.

345

340

Zones of highly porous limestones with visual evidence of cavitation are seen from 0 to -60 m MSL-in drill holes, indicating greater depths than usual in karst-related features in this area. Karstification is common in the KKR and the limestones of the LGG and WAL, as well as along fault zones (McCormack et al., 2017; O'Connell et al., 2018).

Zones of higherelevated velocities ranging from [4000 to 6500 m/s] are present near the surface on the northern and southernmost sidesside of the profile and underlyingbelow the central low-velocity zone (Fig. 6). On the north side of the profile, this corresponds with the presence of the WAL at the surface, which is well-constrained by drilling. Drill hole TC-2638-101 shows similarcomparably elevated laboratory velocities to the velocity model (from 70 to -100 m MSL), ranging from (6000 to 6300 m/s, exhibiting a-) between 70 to -100 m (arrow 3), corresponding to a zone of grey dolomite. These depths correspond to a sequence of within nearly completely dolomitized WAL mud mounds. Similarly, dolomitization also affects WAL mud moundsAt similar depths, in drill hole TC-2638-036 at similar depths. This sequence reveals, dolomitized WAL mud mounds reveal lower velocities (5700 to 6000 m/s), corresponding to associated with a brownish dolomite. This strongly suggests that the tomographic velocity model responds to different dolomitic textures. (arrow 4; Fig. 6). High velocities can also be associated with the stromatactic textures present in the core facies clean zones of the WAL mud mounds, and these are intersected by the drill holes TC-2638-074 and TC-2638-101, displaying velocities of 6000 m/s on both the model and drill holes. These observations strongly suggest that the tomographic velocity model is sensitive to differences in calcite and dolomite textures.

350

355

360

365

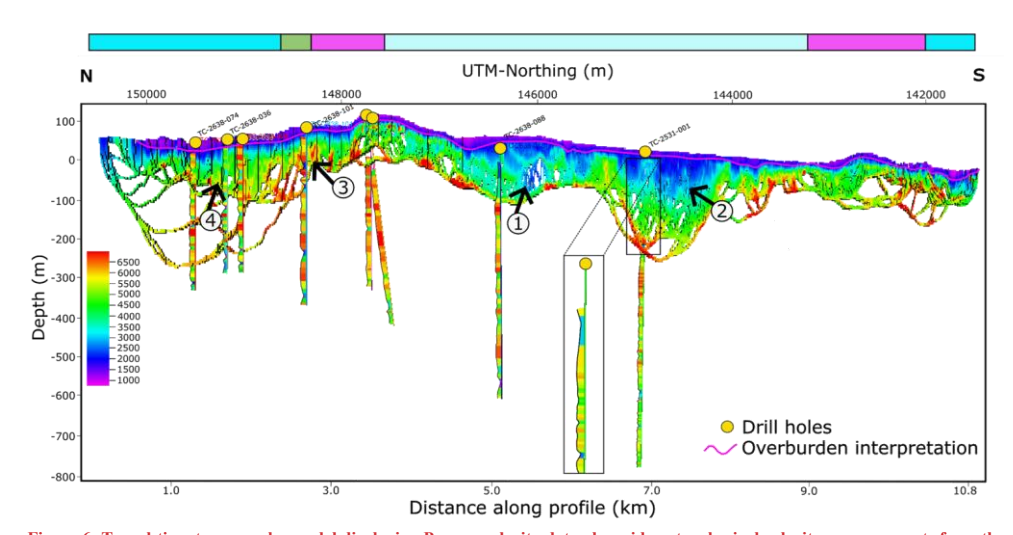


Figure 6: Travel-time tomography model displaying P-wave velocity data alongside petrophysical velocity measurements from the drill core samples (marked by the yellow circles). The purple line outlines the overburden thickness interpreted from the model and drill hole data. Black arrows mark features identified in the model. The coloured top bar represents the bedrock stratigraphy extracted from the geological map.

The velocity model shows interfingered low and moderate velocity zones around 146000mN (Fig. 6(arrow 1), corresponding to 90 meters of altered volcanic sequence of KKR underlain by a dolomitized zone of the LGG intersected by drill hole TC-2638-088. South of 144000mN, the same units are exposed at the surface, with the model revealing a thinner upper low-velocity layer and predominantly high velocities below, indicating a distinct velocity response compared to the northern section of the model. The bedrock geology in this area (Fig. 1) is mapped as KKR.

Younger units (KKS and HBN) are exposed between 146000mN and 144000mN- (arrows 1 and 2; Fig. 6). The response in this portion of the tomography exhibits chaotic behaviour with increased lateral velocity variability, interpreted as interfingering between the volcanic- and limestone-dominated intervals, as supported by drill hole TC-2531-001. The upper 200 meters of this drill hole intersect an interfingered sequence of thickly bedded volcanics, argillaceous limestone, cavities

and basaltic intrusions. Laboratory Vp ranges from 4700 to 6200 m/s, aligning well with velocities observed in G11-2531-01 (Fig. 4a5a), which also intersects KKS, KKR and the limestones of LGG.

## 4.2 Acoustic impedance

375

By combining the <u>P-wave velocity analysis</u> with the density data from the core samples all drill holes, we calculated the acoustic impedance of the main for each data point, as well as an average value for each stratigraphic units and lithological typesunit observed in the drill holes, to identify the main acoustic impedance trends (Fig. 7).

Velocity contrasts between individual units within the Limerick Syncline are generally mild. The most notable differences occur between the WAL and ABL (mean velocities of 6000 vs 5500 m/s, respectively, representing a 10% contrast) and between the LGG and the KKR (mean velocities of 6000 vs 5600 m/s, respectively). These velocity differences are also observed in the downhole Vp logs (Fig. 45). Density contrasts are most prominent between the carbonate and volcanic rocks (approximately 2.7 vs 2.9 g/cm³, respectively) and the carbonate and mineralisation (2.7 vs 3.0 to 4.2 g/cm³, respectively).

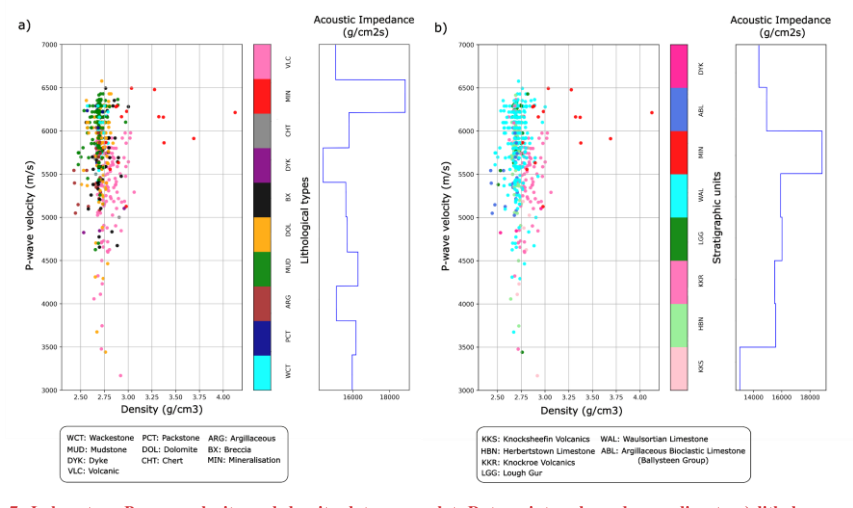


Figure 7: Laboratory P-wave velocity and density data cross-plot. Data points coloured according to a) lithology, and b) main stratigraphic units. The mean acoustic impedance per lithology/unit is outlined in blue.

Formatted: Font color: Auto
Formatted: Font color: Auto

390

380

The ABL exhibits lower acoustic impedances (around impedance (15,000 g/cm²s) than the micritic mudstone samples of the WAL (around-16,500 g/cm²s). This reflects the lithological composition of the upper ABL, containing significant portions of laminated and wavy argillaceous mudstone.mud-rich limestone. Where the two units are juxtaposed, an impedance contrast of 1,000 to 1,500 g/cm²s is expected. However, as seen in G11-2638-06 (Fig. 4b5b), the transition between these units can be gradual, with the top tens of meters of the ABL representing an argillaceous nodulara mudstone-dominant unit with micrite unit oftennodules, which is transitional to the WAL (Somerville et al., 1992). As expected, acoustic impedance in the WAL is highly variable, due to significant variationchanges in density and velocity (Figs. 5 and 7bFig. 7). Most micritic mudstoneclean

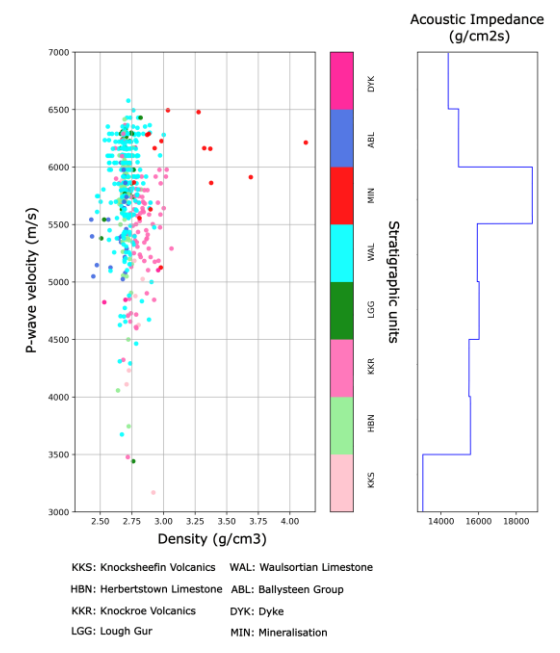


Figure 7: Laboratory P-wave velocity and density data cross-plot. Data points coloured according to main stratigraphic units. The mean acoustic impedance per unit is outlined in blue. Mineralisation and dykes are distinguished in the plot as MIN and DYK, respectively.

samples (Table 4) in the WAL show high acoustic impedance, contrasting with the brecciated and dolomitized samples in the unit  $(\le 15,500 \text{ g/cm}^2\text{s})$ .

The acoustic impedance in the LGG gradually decreases upwards (e.g. G11-2638-06 in Fig. 4b), however5b). However, it is mostly indistinguishable from the WAL. The KKS showshow very low acoustic impedance (around 13,000 g/cm²s). It is characterised by basaltic lava flows, intrusions, and tuffs, representing thick, massive, homogeneous units (Strogen, 1983). Intense chlorite-clay alteration is common in most of the measured KKS samples, typical of extrusive units in both KKS and KKR (Slezak et al., 2023). This may explain the observed low overall acoustic impedance (13,000 g/cm²s) and low velocities (Figs. 4a and Fig. 5a). Basaltic samples of the KKR show much higher acoustic impedance, mainly between 15,000 and 16,000 g/cm²s, and they are distinctly dense (between 2.75 and 3.00 g/cm³; Fig. 7b7). The KKR samples are dominated by relatively unaltered fine-grained massive basalt intrusions, and lower values within KKR (13,500 g/cm²s) correspond to volcaniclastic and tuff samples, which are often altered. The HBN shows very similar behaviour to LGG and WAL, and when interfingered with KKR, does not show notable acoustic impedance contrasts.

Massive sulphide mineralisation shows the highest acoustic impedance values ( $\geq 20,000 \text{ g/cm}^2\text{s}$ ) due to the densities associated with pyrite, sphalerite and galena, with an expected impedance contrast of 4,000 to 5,000 g/cm<sup>2</sup>s for mineralised WAL.

#### 4.3 Seismic reprocessing

400

405

The velocity analysis provided key information to reconstruct the velocity field in the study area, which informed the new stacking velocity model used in both the stack and post-stack time migration.

Based on the picked stacking velocity after analysing the seismic data, a The new stack of lineprofile LK-11-02 was obtained (Fig. 8). The reprocessed seismic image) features areas with prominent reflectivity. The northern part of the profile contains the Stonepark Zn-Pb prospect (Fig. 1), withwhere several drill holes drilledreach depths of up to at least 300 meters (CDPs 0-600). This area is characterised by a group of high—amplitude reflections (R1) with variable geometries and lateral continuity between 100 and 300 ms, exhibiting mound-shaped structures with greater impedance contrasts than those observed right

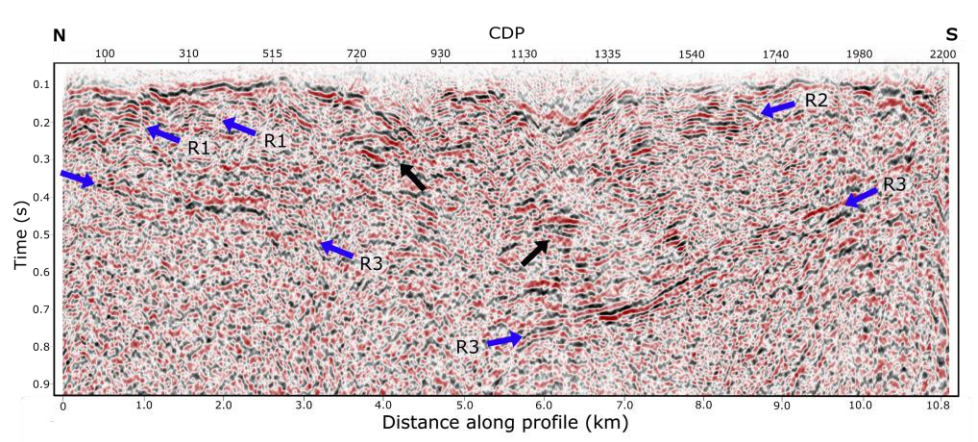


Figure 8: Two-way time stack section with reflections R1, R2 and R3 highlighted by blue arrows. Black arrows indicate discontinuous features identified in the section.

below. Towards the south, a sequence of gently to moderately dipping reflections (R2) shows high amplitude and subparallel to mound-shaped geometries. TheseSimilar reflections are also observed between the CDPs 720 and 1130 and between 1130 and 1335, aroundat 300 to 500 ms (black arrows in Fig. 8).

Laterally continuous reflections (R3) are identified on both sides of the section. The R3 reflections are the deepest continuous reflectors in the profile, below which the reflections become more incoherent. However, there is a significant discontinuity at the central part of the section (between CDPs 720 and 1130), interrupting the R3 package. Notably, these R3 reflectors dip in

Formatted: Don't keep with next

Formatted: Font: 10 pt

opposite directions across this discontinuity (Fig. 8). South of the discontinuity, between CDPs 1130 and 1740, the reflections exhibit good continuity again, with subparallel internal geometries and moderate to steep dips.

#### 5 Discussion

420

125

The acquisition and processing 5.1 Impact of additional velocity field information provided a key hitherto missing step, enabling petrophysics-guided seismic reprocessing on seismic imaging of legacy data in the Limerick Syncline. The Vp data collected from drill holes along the profile LK-11-02 and

To evaluate the impact of our reprocessing on the imaging of profile LK-11-02, we compared the results of the travel-time tomography presented insights into the P-wave velocity of the mainKirchhoff post-stack time migration with the Kirchhoff pre-stack time migration of dataset 2 (Fig. 9). Reflections recovered by the pre-stack time migration (Fig. 9a) are mainly concentrated in the shallow subsurface between 100 and 200 ms, where reflections R1 and R2 (mapped in Fig. 8) appear only partially imaged and with chaotic patterns. In contrast, in the post-stack time migration (Fig. 9b), R1 is expressed as mound-shaped reflections and R2 as subparallel reflections. The R3 package is visible in the southern part of the profile (south of CDP)

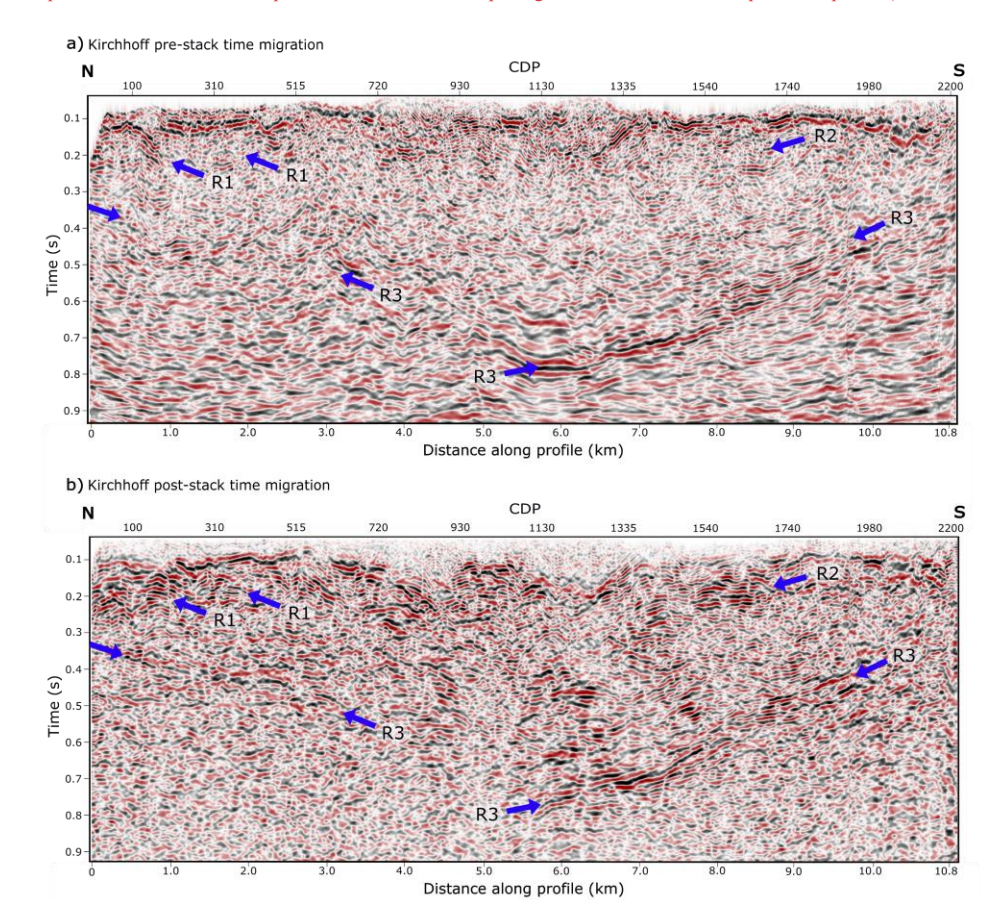


Figure 9: Two-way time migrated sections from dataset 2 and new reprocessing, a) Kirchhoff pre-stack time migration from dataset 2, and b) new Kirchhoff post-stack time migration. Reflection R1, R2 and R3 are highlighted by blue arrows.

Formatted: Font: Bold, Font color: Auto

1130) in both migrations, with relatively good continuity. However, the pre-stack migration struggles to resolve reflections on the north side of the section below 200 ms, producing migration smiles.

The use of an updated velocity model, combined with stacking before time migration, improved the signal-to-noise ratio by mitigating and reducing the effects of the noisy CMP gathers and complex geology. This resulted in better signal recovery in both the shallow and deep portions of the section, revealing enhanced continuity and previously unresolved reflections of geological units of the shallow part of the study area, allowing us to improve and reinterpret the seismiesignificance. Overall, the reprocessed and newly migrated section sharpens reflector geometries and amplitude variations, making the image—more interpretable.

5.12 Seismic interpretation

130

135

140

445

150

455

160

Figure 9e10 shows an integrated seismicthe interpretation of the main stratigraphic units and structures, with time-converted drill holes containing on a depth-converted profile LK-11-02. The post-stack time-migrated section was depth-converted using a constant velocity of 5500 m/s, with the datum set at 160 m MSL. Drill holes projected onto the section provide geological logging information highlighting formations, control, documenting dolomitization, brecciation, argillaceousmud-rich intervals and dyke intrusions. The blackBlack dashed lines outline the interpretation of previously unknowninterpreted major faults F1 and F2. The coloured top bar represents the bedrock stratigraphy extracted from the geological map (Geological Survey Ireland, 2022), not previously mapped in the region.

The reflections R3 are interpretedattributed to represent the LLS Group (yellow horizon in Fig. 9e10b), comprising interbedded cross-bedded sandstones, oolitic and skeletal grainstones and fissile shales with desiccation cracks (Somerville & Jones, 1985; Somerville et al., 2011). This heterolithic sequence could explain the observed seismie facies of a high-amplitude, subparallel, continuous package of reflectors. The topupper contact of these reflections R3 is interpreted as the contact between the transition from mixed siliciclastic-carbonate-evaporite sequence and the sequences to fully marine open ramp carbonate-dominated ramp sequences, likely corresponding to of the more argillaceous Ballymartin Formation, but certainly including the and Ballysteen Formation (Somerville and Jones, 1985).

The enhanced continuity of reflections and the geological combined with drilling constraints from drilling data atin the northern portion of the section facilitated the interpretationallows recognition of the ABL-WAL contact between the ABL and the WAL (outlined by the (dark-blue horizon in Fig. 9e10b). The overlying zone (WAL) exhibits high-amplitude, mound-shaped structures with greater impedance contrasts than those observed right below (between 100 and 300 ms)<sub>12</sub> corresponding with the observed Vp\_variability in Vp with different facies within the WAL<sub>7</sub> (Fig. 7; Table 4).

Internal form lines within the WAL earbonate rocks (cyan blue in Fig. 9e) highlight various geometries outlined by 10b) outline semi-continuous moderate to high amplitude reflectors. These semi-continuous reflectors show reflections in mound-shaped geometries with opposing dipdips, and associated onlap and offlap terminations. These features correlate well with changes in facies of the WAL mud mounds astransitions observed in drill holes in Fig. 9e. Transition from core mudbank facies to flank facies correlates with increased reflectivity. The cores of the (Fig. 10b), from massive micritic mud mound consist of massive micrite mudstone, with cores (higher acoustic impedance, and the mud mound flanks consist of higher) to bioclastic content with rich flanks containing variable amounts of clay, with mud (lower acoustic impedance (Fig. 7). Outcrops studies). Outcrop and drill datacore evidence across the Irish Midlands clearly show that individual WAL mud mounds can have dimensions of tens to a few hundred meters in thickness (Lees, 1964) with amalgamated mud mound complexes extending laterally for kilometres (Devuyst and Lees, 2001), especially in the Limerick area (Somerville et al., 20122011).

**Formatted:** Border: Top: (No border), Bottom: (No border), Left: (No border), Right: (No border), Between: (No border)

Formatted: Don't keep lines together

The veryDistinctive high\_amplitude and reflection patterns in Fig. 10 are generally associated with igneous rocks. North of CDP 720, shallow, laterally continuous quasi-horizontal shallowsubparallel reflectors seen north of CDP 720 at ~\_100 msm (dark pink dashed form line; Fig. 9e),10b) coincide well—with observed low angle basaltic dykes, as well asintrusions that interfinger with thick (≥ 50 meters) argillaceous rich—WAL mud mound flank facies in TC-2638-101, (≥ 50m), and thick argillaceouswith flank facies with minor dykes in TC-2638-026 and TC-2638-036. (Fig. 4).

Towards To the south, several high-amplitude, semi-continuous quasi-horizontal subparallel reflectors, like the (e.g. R2 reflections (; Fig. 8), were 9b) are interpreted as KKR units (dark pink form lines (; Fig. 9e), representing the KKR-10b). These

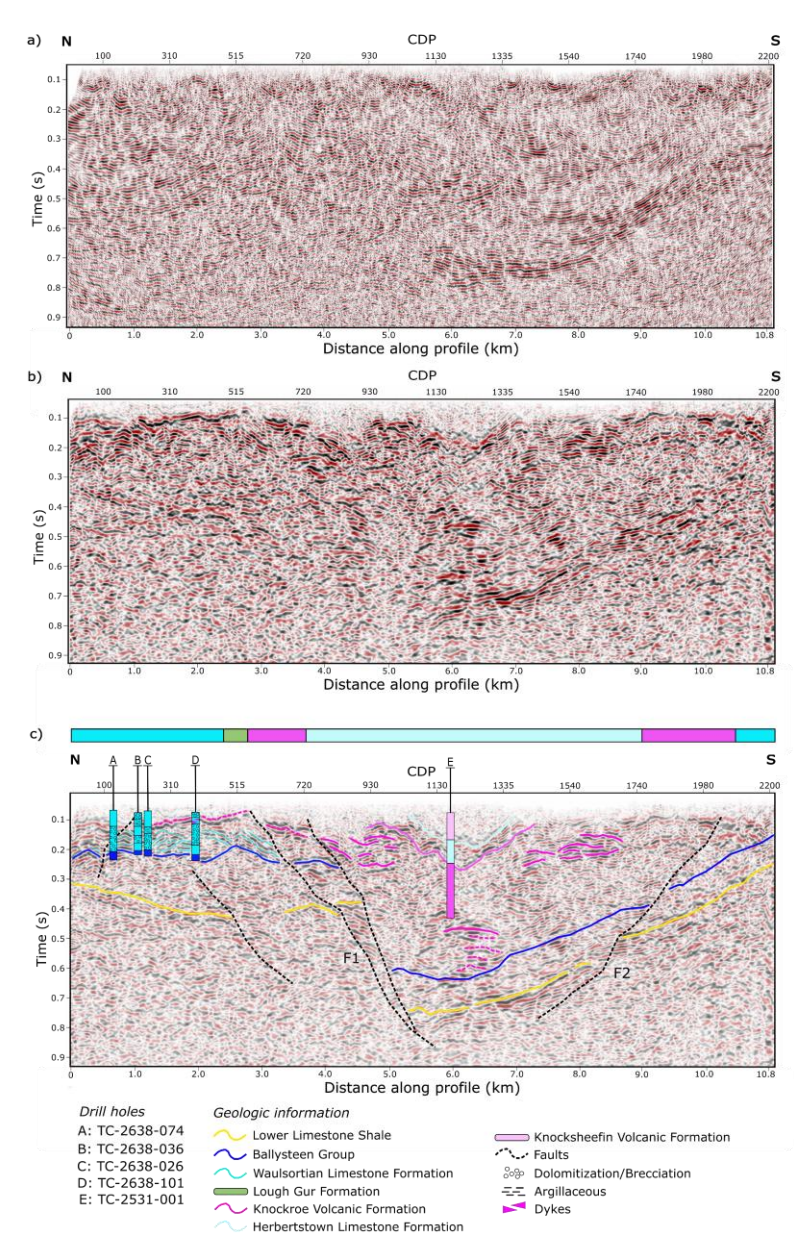


Figure 9: Legacy dataset 1 and new processing migrated sections. a) Legacy phase-shift post-stack time migration and b) new kirehhoff post-stack time migration. (c) Seismie interpretation of the main stratigraphic units with time-converted drill holes containing geological logging information (units and textures—dolomitization/brecciation, argillaceous intervals and dyke intrusions). Interpretation of faults F1 and F2 are outlined by black dashed lines. The coloured top bar represents the bedrock stratigraphy extracted from the geological map

strong reflectors are often underlain by extensive vertically connected zones of moderate to high amplitude but discontinuous reflectivity, rooting extending down for up to 600 ms. Laterally, these reflections are ~ -1500 m, and interfingering with chaotic

reflections of lower, low amplitude reflections. The KKR comprises abundant basaltic maar-diatremes, lava flows, intrusions, tuffs and volcaniclastic units (Strogen, 1983; Elliott et al., 2015; Slezak et al., 2023). The In this context, the high-amplitude, mound-shaped reflections between CDPs 1130 and 1335 are therefore interpreted as an example of an intrusion (intrusive complex, possibly a diatreme pipe andwith associated intrusives) associated with the KKR. The surrounding chaotic low-amplitude reflections between 150 and 400 ms are interpreted as interfingering between the different 250 and -900 m likely represent volcanic rocks and the carbonate rocks of interfingering within the LGG and HBN.

The contact between the KKS and the HBN is constrained by the drill hole TC-2531-001 and outlined by the light-greenblue horizon (Fig. 9e10b). The acoustic impedance plot (Fig. 7) exhibits low values for the altered volcanic samples, tuffs, and volcaniclastics and high values for basaltic lava flows, reinforcing the contrasts observed in the seismic section.

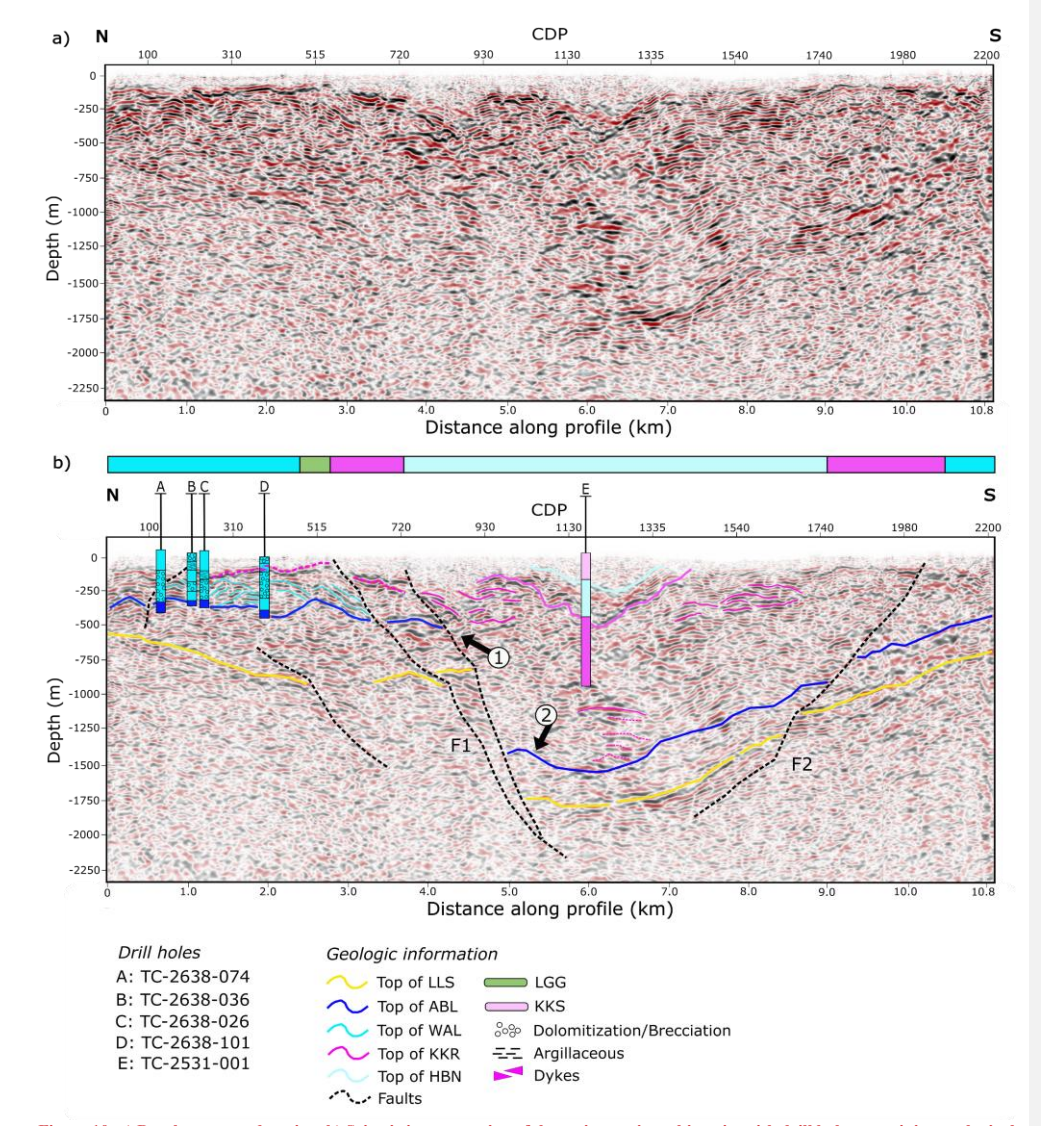


Figure 10: a) Depth-converted section. b) Seismic interpretation of the main stratigraphic units with drill holes containing geological logging information (units and textures - dolomitization/brecciation, argillaceous intervals and dvke intrusions). Interpretation of faults F1 and F2 are outlined by black dashed lines. Arrows 1 and 2 indicate features identified in the section. The coloured top bar represents the bedrock stratigraphy extracted from the geological map.

Several interpreted faults crosscut the section. A significant discontinuity interrupts—the continuity and elevation of the LLS package. This is interpreted as a major south-dipping (segmented) fault (F1) displacing the LLS by approximately 450 ms.750 m. Additionally, a north-dipping fault (F2) is interpreted to the south of F1, displacing the LLS by approximately 100 ms.200 m. Reflectors of overlying units are dipping north towards F1, forming a clear normal fault half-graben geometry, with F1 representing a terraced fault system. Several antiformal geometries and domed reflections (arrow 2) are observed in the immediate hanging wall and footwall of the fault, as well as in the F1 fault blocks. A zone of more steeply dipping LLS

reflectors is also seen between CDPs 1540 and 1740. These are interpreted as representing inversion geometries, possibly associated with the Variscan Orogeny,

Formatted: Font color: Auto

#### 5.2 Legacy and new processing

490

495

500

505

510

515

520

**\$**25

To assess the impact of the updated velocity model on the imaging of profile LK-11-02, the results of the new Kirchhoff post-stack time migration (Fig. 9b) are compared against the legacy dataset 1, which consists of a phase-shift post-stack time migration (Fig. 9a).

The new post-stack time migration demonstrates good signal recovery in both the shallow and deep portions of the section, revealing enhanced continuity and previously unresolved reflections of geological significance. While the legacy phase shift time migration exhibits parts of reflections like R1, between CDPs 100 and 200, and R3 at 400 ms, it struggles to resolve other reflections recovered in the new processing. Reflections R3 are visible in the southern part of the profile (south of CDP 1130) in both workflows, with good continuity. Moderately dipping reflectors between CDPs 1540 and 1740, within two-way times of 400 to 500 ms, are well imaged in the legacy migration (Fig. 9a), but lose continuity in the new processing. Despite this, similar onlap terminations are evident in both images near CDP 1540. Apparent migration smiles in the legacy image are collapsed in the new processing, leading to improved imaging, particularly in the shallow zones below the KKS (Figs. 9b and 9e). Overall, the new migrated section enhances reflector geometries and amplitude variations, making the image more interpretable.

#### 5.3 Implications for mineral exploration

#### 5.3 Imaging potential of Zn-Pb deposits and surrounding hydrothermal breccias

According to Salisbury et al. (2000), a sulphide deposit can be imaged using seismic if it meets three conditions: i) a sufficiently high reflection coefficient (R), specifically greater than 0.06 in their study; ii) a diameter greater than the width of the Fresnel zone; and iii) a thickness of at least ¼ wavelength due to seismic vertical resolution.

In our study, although the Zn-Pb mineralisation in the Limerick Syncline has a sufficiently high reflection coefficient and Fresnel zone, it is unlikely to be directly imaged due to its moderate thickness. The mineralisation typically occurs in 10-meter intervals within brecciation zones in the WAL, below the vertical resolution of the seismic data (, estimated at approximately 40 meters). for a dominant frequency of 40 Hz. However, our acoustic impedance study indicates that the mineralisation exhibits the highest impedance values compared to the main lithologies in the area (Fig. 7). This suggests that if a sphalerite/galena-rich zone extended laterally for at least 240 meters (approximate Fresnel zone width) and had a minimum thickness of 36 meters, it could potentially be imaged by the seismic (calculations assume Vp = 5800 m/s, dominant frequency = 40 Hz, and a depth of= 200 meters).

Breeciation zones are also extensively present in the Stonepark WAL, showing Hydrothermal dissolution-precipitation breecias are widely associated with Zn-Pb mineralisation in the Irish Midlands (Hitzman, 1999; Wilkinson et al., 2011; Güven et al., 2023) and are also recognised at Stonepark and Pallas Green (Elliott et al., 2019; Blaney and Coffey, 2023). At Stonepark, breeciation zones within the WAL display lower acoustic impedance values compared to unaltered carbonate samples (Fig. 7). This contrasts with the seismic characteristics of WAL mud mounds. Drill holes intersected breecias intersect WAL breecia zones between CDPs 100 and 515, within two-way times of at depths from -100 and 200 ms (Fig. 9c), providing constraints for the seismic interpretation. These breeciated zones coincide to -300 m (Fig. 10b), coinciding with a chaotic, low-amplitude seismic facies. Delomitization occurs in the same area at different intervals, however, its seismic facies This contrasts with the

seismic characteristics of WAL mud mounds (Fig. 10b) and dolomitization, whose seismic responses closely resemble theorems that of the mud mounds.

The distinctive seismic facies observed incharacter of these brecciated zones, as confirmed by drilling, therefore highlights thetheir potential for using brecciation as a seismic proxy for indirect seismic proxies for potential Zn-Pb mineralisation. Our work suggests that directly incorporating breccia identification into seismic interpretation may sharpen drill targeting mineralisation. This approach could also support drilling campaign planning. To further evaluate its effectiveness, we will apply this reprocessing workflow to the other five Stonepark and Pallas Green seismic profiles in the future.

The occurrence of breccias and mineralisation at Stonepark and Pallas Green also ties into the structural framework (Blaney and Coffey, 2023). Given the proximity of the Stonepark deposit to fault F1, the structure could have acted as a master conduit for metal-bearing fluids within the overall mineral system (Torremans et al., 2018; Walsh et al., 2018), penetrating deeply into the Lower Palaeozoic basement rocks, the source of metals for mineral systems in the Irish Orefield (Johnston et al., 1999; Wilkinson, 2023). In addition, the presence of significant displacement on F2 in the southern side of the section (Fig. 10b) suggests it could also have served as a hydrothermal fluid pathway, further opening exploration search space on the opposite flank of the Limerick Syncline.

## 5.4 Implications for the architecture of the Limerick Syncline

530

35

545

550

555

560

The Limerick Syncline forms a regional ovoid-shaped map pattern whose structural evolution remained poorly understood. The Stonepark and Pallas Green deposits, located in the northwest portion of the Syncline, are crosscut by a series of small throw, north-northwest-striking faults that appear to locally control the distribution of mineralisation (Blaney and Coffey, 2023) but which lack demonstrable growth sequences. However, the main basin-controlling and potentially ore-controlling normal faults remained unidentified in the study area (Blaney and Redmond, 2015). A key implication of the new processing is that such major faults (F1, F2) are now clearly identified Our velocity analysis and seismic reprocessing approach have identified a major south-dipping fault (F1) and a north-dipping fault (F2) to the south of Stonepark and Pallas Green.

A considerable change in Considerable thickness is variations are observed in the stratigraphy from north to south of the along profile LK-11-02 (Fig. 910). The units are crosseut by various faults along the section (Fig. 9e), including the major south-dipping fault (F1) and the north-dipping fault (F2). No Tournaisian units, LLS and ABL, appear to show no significant thickness changes are observed in the Early Mississippian units, LLS and ABL. However, the thickening of the change, consistent with their depositional setting as a shallow-marine, tidally influenced environment on an inner ramp, grading upward into more mud-dominated shelf/ramp conditions that precede WAL buildups (Somerville and Jones, 1985; Somerville et al., 1992). They are therefore interpreted to be largely deposited in a pre-rift setting. In contrast, the WAL, LGG, and KKR volcanic sequence thicken in the hanging wall of F1-indicates potential, implying syn-depositional fault activitygrowth during the Late Tournaisian to Early Viséan, corresponding to the KKR and KKS emplacement (Slezak et al., 2023). This timing is alsolate Tournaisian to early Viséan. Together, F1 and F2 form a half-graben geometry, which has not previously been recognised or described for the Limerick Basin. These fault growth timings are consistent with those observed in the northern and central Midlands of Ireland, where faults are suggested to have been active during from the Uppermiddle Tournaisian and have influenced, significantly influencing basin and mineralisation-development from the Viséan onward (Johnston et al., 1996; Hitzman, 1999; de Morton et al., 2015; Ashton et al., 2018). There, coincident mineralisation was caused by hydrothermal fluid flow along the developing fault systems (Torremans et al., 2018; Güven et al., 2023).

Formatted: Font color: Red

The south-dipping fault (F1) displaysexhibits two fault strands bifurcating from a common point at depth, suggesting a segmented normal fault geometry-showing, with gentle rotation of the reflectors (arrow 1, Fig. 10b) between the two interpreted segments (CDPs 515 to 930). At These are similar in nature to normal fault arrays observed elsewhere in the Irish Midlands (Kyne et al., 2019) and, therefore, strongly indicate that large-scale relay ramp geometries are present in the Limerick Syncline (Walsh et al., 2018), increasing the likelihood that further significant normal faults are to be identified in the region. In the hanging wall and footwall of F1, domed reflections (arrow 2, Fig. 10b) are interpreted as representing inversion geometries (Bonini et al., 2012)). These are likely associated with the Variscan Orogeny-deformation, which led to regional north-south compression and consequent basin inversion, reactivating normal faults and producing reverse faulting (Meere, 1995; Fusciardi et al., 20042003; Kyne et al., 2019). Similar domed geometries are also observed on the south side of the profile, dipping towards fault F2. These geometries indicate the impact of the compressional event in the Limerick Syncline. This observation of significant inversion tectonics on km-scale normal faults, and its confluence at the edge of the present-day Limerick Syncline, explains why these Mississippian normal faults have hitherto not been recognised, since current net displacements on F1 are mostly reverse at present-day erosion levels.

In addition to identifying faults, the new processing has also enhanced our understanding of the distribution of the volcanic sequence along the seismic profile, which shows some association with faulting. The interpreted low-angle-basaltic dykesintrusions, located north of CDP 720 (Fig. 9e10b), are interrupted by the segmented fault (F1). This high-amplitude reflector package reveals an increased thickness between CDPs 515 and 720, in comparison compared to the geometry observed north of CDP 515, suggesting the coeval timing of faulting and volcanism in the region; both culminating during the Viséan. High-amplitude and laterally continuous quasi-horizontal subparallel shallow reflectors, such as those linked to the basaltic dykesintrusions, are also noted south of CDP 1740 around at a depth of 100 msm, intersected by fault (F2). This indicates that the southern side of the profile displays a geological setting very similar to that of the northern side, where the Stonepark deposit is situated.

#### 5.5 Velocity analysis

The P-wave velocity shown in Fig. 6, from travel-time tomography, details the near-surface of both sides of the Limerick Syncline. The low velocity zone associated with the overburden and karstification on the north side shows greater thickness than the south side, which shows a more rapid increase in velocity. However, thickening of this low velocity zone is observed towards the end of the profile, south of 142000mN, which potentially indicates limestone or fault-related karstification. The performed velocity analysis showed that the Waulsortian Limestone Formation can be very complex due to its variable lithologies and consequent wide range of velocities, which is controlled by the mud mound facies, clay content, dolomitization, brecciation and mineralisation. As confirmed by the drill hole data, the dolomitization is widespread in the Stonepark deposit and replaces extensive areas of the Waulsortian Limestone, influencing the velocity model. Coincidentally with Stonepark, we observe lower velocities in the model where drill holes intersected intense dolomitization and brecciation, processes that can decrease Vp as seen in the petrophysics data.

This interpretation is more challenging on the south side of the profile because of the absence of drill holes. The rapid increase in velocity in areas predominantly composed of Waulsortian Limestone could indicate either the presence of clean micritic Waulsortian or high-velocity dolomite. The same lateral velocity contrast of high and moderate velocity zones seen between 150000 and 148000mN on the north side, coinciding with different dolomite textures and brecciated zones in Stonepark, is also seen between 144000 and 142000mN on the south side of the velocity model. Interestingly, the south side of the seismic section suggests the presence of a major north-dipping fault (Fig. 9c), which could have acted as a hydrothermal fluid conduit, emplacing mineralisation in the WAL on the opposite flank of the Limerick Syncline.

#### 6 Conclusions

605

310

315

320

325

630

35

640

This study demonstrates the impact of how selecting an appropriate propriately tailored processing workflow and integrating, guided by geological and petrophysical data-on-enhancing legacy, can substantially enhance seismic data-interpretation. Incorporating additional datasets, such as drilling information, downhole and laboratory P-wave velocity measurements, and travel-time tomography into the stacking velocity model and post-stack migration has improved the subsurface imaging of theon profile LK-11-02, sharpening continuity and fidelity of reflectors. The velocity and acoustic impedance analysis provided valuable insights into the imaging potential of unit boundaries, brecciation zones and mineralisation. The reprocessed seismic section improved the interpretability of lateral lithology changes, such as the interfingering of volcanic and carbonate rocks and fault zones, previously considered gaps in the subsurface understanding of the area. We interpreted a south dipping fault zone, which can be part of the conduits that provided the mineral system with metal-bearing hydrothermal fluids. And, from the acoustic impedance analysis, we observed that the mineralisation has a high reflection coefficient. However, in the Limerick Syncline, the mineralised intervals are not thick enough to be directly imaged with the available seismic data resolution.

Furthermore, this study raises considerations regarding the southeastern side of the Limerick Syncline, where seismic data revealed a major north-dipping fault, and similarities in velocity distribution observed in the travel-time tomography suggest a potentially similar setting of the carbonate rocks, emphasising the need for further investigation with a focus on mineralisation potential.

The reprocessed seismic section resolves key stratigraphic and facies architecture previously obscured, including the ABL-WAL contact, internal WAL mud mound form lines, and the lateral interfingering of volcanic (KKR/KKS) and carbonate (LGG, HBN) units. Importantly, we identify two previously unmapped, basin-scale structures: a south-dipping segmented normal fault (F1) and a north-dipping fault (F2) that together bound a syn-rift (half-)graben geometry. Their geometry and associated reflection patterns are consistent with late Tournaisian to early Viséan syn-depositional faulting during Mississippian rifting, coeval with emplacement of the Limerick Igneous Suite, and followed by Variscan inversion tectonics, which provide net zero displacements at the present-day surface. Given its position near Stonepark, the south-dipping F1 is a plausible hydrothermal fluid conduit for the mineral system. Furthermore, this study highlights that the southern side of the Limerick Syncline, where our new imaging workflow reveals a major north-dipping fault, F2, warrants follow-up investigation.

From the acoustic impedance analysis, sulphide mineralisation exhibits high reflection coefficients. However, the typical 10 m-thick intervals are below the quarter-wavelength vertical resolution necessary to be directly imaged at ~ 200m depth with the available seismic data. Consequently, direct seismic imaging of similar discrete sulphide bodies as known in the Limerick Syncline is unlikely. However, WAL breccia corridors, often surrounding Zn-Pb mineralisation, display lower acoustic impedance and are mapped as chaotic, low-amplitude seismic zones, confirmed by drill hole intersections. Where these corridors are laterally extensive, they may provide a practical indirect seismic proxy for Zn-Pb targeting.

Lastly, the workflow explored in this study presents a cost-effective and transferable approach forto mineral exploration. By revisiting the legacyre-evaluating seismic data and integrating complementary techniques into the reprocessing with added petrophysics, valuable new geological insights can be extracted, offering an alternative to, or supporting the decision to, acquire new seismic data. Moreover, this approach enables the recovery of additional geological information from datasets that required significant financial and operational effort to acquire, thus contributing to the revalorisation of existing resources and maximising their exploratory potential.

#### Data availability

Seismic data underpinning this work can be requested through the Geoscience Regulation Office (GSRO) of the Department of the Environment, Climate and Communications of the Government of Ireland. The petrophysics data generated in this work can be obtained upon request from the authors—and will be. Measurement metadata reports per drill hole are published in a research repository (Zenodo). Other complementary data can be obtained from the authors upon request.

#### **Author contributions**

650

655

660

VS: conceptualisation, petrophysical data acquisition, seismic, tomography and petrophysical data processing, data interpretation and integration, writing (original draft preparation) and editing; AM: conceptualisation, project management, supervision, funding acquisition, reviewing; KT: conceptualisation, data interpretation and integration, supervision, reviewing; JA: seismic processing methodology, supervision, reviewing; DM: travel-time tomography methodology, supervision, reviewing; RB: seismic processing methodology, reviewing.

#### Competing interests

The authors declare that they have no conflict of interest.

#### Acknowledgements

We greatly thank Group Eleven Resources, particularly Mark Holdstock and Sean Walsh, for providing geological logging data and drill core samples used in this study for laboratory petrophysical measurements, as well as for valuable geological discussions. We also acknowledge Robertson Geo for downhole petrophysics data acquisition. We are grateful to Glenn Morgan, Earth Signal Processing, and VelSeis Processing for providing the legacy seismic datasets used in the new processing discussed in this study. Additionally, we appreciate AspenTech, RadExPro and SLB for granting academic licenses for their software, which is used as the main tool in seismic processing. Special thanks to Philip Rieger and Eoin Dunlevy for their invaluable support in geological discussions. Finally, we extend our gratitude to the Geological Survey-of Ireland for hosting the UCD Petrophysics Laboratory from 2021 to 2023 and to research assistants Conor Farrell, Eoin Byrne and Gabriel Cavalcanti for their valuable support in the petrophysics laboratory.

# 665 Financial support

This research was partly supported by a UCD Ad Astra Studentship and partly supported by Science Foundation Ireland, now Research Ireland, projects 13/RC/2092\_P2 and 16/RP/3849. JA and DM acknowledge funding from the VECTOR project; this research has received funding from the European Union's Horizon Europe research and innovation programme under grant agreement no.101058483 and from UK Research and Innovation.

## 670 References

Alcalde, J., Carbonell, R., Pospiech, S., Gil, A., Bullock, L.A. and Tornos, F., 2022. Preface: State of the art in mineral exploration. *Solid Earth*, 13(7), pp.1161-1168.

Ali, S.H., Giurco, D., Arndt, N., Nickless, E., Brown, G., Demetriades, A., Durrheim, R., Enriquez, M.A., Kinnaird, J., Littleboy, A. and Meinert, L.D., 2017. Mineral supply for sustainable development requires resource

675	governance. Nature, 543(7645), pp.367-372.
	Ashton, J.H., Beach, A., Blakeman, R.J., Coller, D., Henry, P., Lee, R., Hitzman, M., Hope, C., Huleatt-James, S., O'Donovan,
	B. and Philcox, M.E., 2018. Discovery of the Tara Deep Zn-Pb Mineralization at the Boliden Tara Mine, Navan, Ireland:
	Success with Modern Seismic Surveys.
	Bell, T., Turner, G., Bhat, G. and Knell, B., 2023, August. Multiscale insights into the Mount Weld REE deposit from 2D and
680	3D active seismic survey data. In SEG International Exposition and Annual Meeting (pp. SEG-2023). SEG.
	Benz, H.M., Chouet, B.A., Dawson, P.B., Lahr, J.C., Page, R.A. and Hole, J.A., 1996. Three-dimensional P and S wave
	velocity structure of Redoubt Volcano, Alaska. Journal of Geophysical Research: Solid Earth, 101(B4), pp.8111-8128.
	Blaney, D. and Redmond, P.B., 2015. Zinc-lead deposits of the Limerick Basin, Ireland. Current Perspectives on Zinc
	Deposits, pp.73-84.
685	Blaney, D. and Coffey, E., 2023. The volcano-stratigraphic setting of the Pallas Green Zn-Pb deposit, County Limerick The
	volcano-stratigraphic setting of the Pallas Green Zn-Pb deposit, County Limerick. In: Andrew, C.J., Hitzman, M.W. &
	Stanley, G. Irish-type Deposits around the world, Irish Association for Economic Geology, Dublin, pp. 285-308. DOI:
	https://doi.org/10.61153/QHKU2937
	Bonini, M., Sani, F. and Antonielli, B., 2012. Basin inversion and contractional reactivation of inherited normal faults: A
690	review based on previous and new experimental models. Tectonophysics, 522, pp.55-88.
	Cheraghi, S., Hloušek, F., Buske, S., Malehmir, A., Adetunji, A., Haugaard, R., Snyder, D. and Vayavur, R., 2023. Reflection
	seismic imaging across a greenstone belt, Abitibi (Ontario), Canada. Geophysical Prospecting, 71(7 Special Issue: Mineral
	Exploration and Mining Geophysics), pp.1096-1115.
	Chew, D.M., Stillman, C.J., Holland, C.H. and Sanders, I.S., 2009. Late Caledonian orogeny and magmatism. The Geology of
695	<i>Ireland</i> , 2, pp.143-173.
	de Morton, S.N., Wallace, M.W., Reed, C.P., Hewson, C., Redmond, P., Cross, E. and Moynihan, C., 2015. The significance
	of Tournaisian tectonism in the Dublin basin: implications for basin evolution and zinc-lead mineralization in the Irish
	Midlands. Sedimentary Geology, 330, pp.32-46.
	de Morton, S., Wallace, M.W., Reed, C., Hewson, C., Redmond, P., Cross, E. and Moynihan, C., 2015. The value of a
700	$ {\color{red} \textbf{combined approach: Innovative mineral exploration techniques in the Irish Zn-Pb ore field.} \textit{ASEG Extended Abstracts}, 2015 (1), \\ {\color{red} \textbf{combined approach: Innovative mineral exploration techniques in the Irish Zn-Pb ore field.} \textit{ASEG Extended Abstracts}, 2015 (1), \\ {\color{red} \textbf{combined approach: Innovative mineral exploration techniques in the Irish Zn-Pb ore field.} \textit{ASEG Extended Abstracts}, \\ {\color{red} \textbf{combined approach: Innovative mineral exploration techniques in the Irish Zn-Pb ore field.} \textit{ASEG Extended Abstracts}, \\ {\color{red} \textbf{combined approach: Innovative mineral exploration techniques in the Irish Zn-Pb ore field.} \textit{ASEG Extended Abstracts}, \\ {\color{red} \textbf{combined approach: Innovative mineral exploration techniques in the Irish Zn-Pb ore field.} \textit{ASEG Extended Abstracts}, \\ {\color{red} \textbf{combined approach: Innovative mineral exploration techniques in the Irish Zn-Pb ore field.} \textit{ASEG Extended Abstracts}, \\ {\color{red} \textbf{combined approach: Innovative mineral exploration techniques in the Irish Zn-Pb ore field.} \textit{ASEG Extended Abstracts}, \\ {\color{red} \textbf{combined approach: Innovative mineral exploration techniques in the Irish Zn-Pb ore field.} \textit{ASEG Extended Abstracts}, \\ {\color{red} \textbf{combined approach: Innovative mineral exploration techniques in the Irish Zn-Pb ore field.} \textit{ASEG Extended Abstracts}, \\ {\color{red} \textbf{combined approach: Innovative mineral exploration techniques in the Irish Zn-Pb ore field.} \textit{Association techniques}, \\ {\color{red} \textbf{combined approach: Innovative mineral exploration techniques in the Irish Zn-Pb ore field.} \textit{Association techniques}, \\ {\color{red} \textbf{combined approach: Innovative mineral exploration techniques in the Irish Zn-Pb ore field.} \textit{Association techniques}, \\ {\color{red} \textbf{combined approach: Innovative mineral exploration techniques}, \\ {\color{red} $
	<del>pp.1-4.</del>
	Devuyst, F.X. and Lees, A., 2001. The initiation of Waulsortian buildups in Western Ireland. Sedimentology, 48(5), pp.1121-
	<del>1148.</del>
	Eaton, D.W., Milkereit, B. and Salisbury, M., 2003. Seismic methods for deep mineral exploration: Mature technologies
705	adapted to new targets. The leading edge, 22(6), pp.580-585.
	Eaton, D.W., Adam, E., Milkereit, B., Salisbury, M., Roberts, B., White, D. and Wright, J., 2010. Enhancing base-metal
	exploration with seismic imaging. Canadian Journal of Earth Sciences, 47(5), pp.741-760.
	Eberli, G.P., Baechle, G.T., Anselmetti, F.S. and Incze, M.L., 2003. Factors controlling elastic properties in carbonate
	sediments and rocks. The Leading Edge, 22(7), pp.654-660.
710	Elliott, H.A.L., Gernon, T.M., Roberts, S. and Hewson, C., 2015. Basaltic maar diatreme volcanism in the Lower
	Carboniferous of the Limerick Basin (SW Ireland). Bulletin of Volcanology, 77, pp.1-22.
	Fusciardi, L.P., Guven, J.F., Stewart, D.R.A., Carboni, V., Walsh, J.J., Kelly, J.G., Andrew, C.J., Ashton, J.H., Boland, M.B.,
	Earls, G. and Fusciardi, L., 2003. The geology and genesis of the Lisheen Zn-Pb deposit, Co. Tipperary, Ireland. Europe's
	major base metal deposits, pp.455-481.
715	$\underline{Geological  Survey  of  Ireland, 2022, Bedrock  geology  of  Ireland  map  1:100,000: Limerick  Basin,  Geological  Survey  of  Ireland.}$

	eentral Sweden. Ore Geology Reviews, 137, p.104306.
	Gordon, P., Kelly, J. G. and van Lente, B., 2018. NI 43-101 Independent Report on the Zinc-Lead Exploration Project
720	Stonepark, County Limerick, Ireland. www.groupelevenresources.com/I
	<del>jects/Stonepark.</del>
	Hitzman, M.W., 1999. Extensional faults that localize Irish syndiagenetic Zn-Pb deposits and their reactivation during Varis
	compression. Geological Society, London, Special Publications, 155(1), pp.233-245.
	Hool, A., Helbig, C. and Wierink, G., 2024. Challenges and opportunities of the European critical raw materials act. Mine
725	Economics, 37(3), pp.661-668.
	Johnston, J.D., Coller, D., Millar, G. and Critchley, M.F., 1996. Basement structural controls on Carboniferous-hosted by
	metal mineral deposits in Ireland. Geological Society, London, Special Publications, 107(1), pp.1-21.
	Johnston, J.D., 1999. Regional fluid flow and the genesis of Irish Carboniferous base metal deposits. <i>Mineralium Deposita</i> , pp.571-598.
730	Kyne, R., Torremans, K., Güven, J., Doyle, R. and Walsh, J., 2019. 3-D modeling of the lisheen and silvermines depos
	County Tipperary, Ireland: insights into structural controls on the formation of Irish Zn-Pb deposits. <i>Econo</i>
	Geology, 114(1), pp.93-116.
	Lees, A.L.A.N., 1964. The structure and origin of the Waulsortian (Lower Carboniferous) "reefs" of west-cen
	Eire. Philosophical Transactions of the Royal Society of London. Series B, Biological Sciences, 247(740), pp.483-5
735	Lees, A. and Miller, J., 1995. Waulsortian banks (Vol. 23, pp. 191-271). Oxford, UK: Blackwell Po
	Liberty, L.M., Schmitt, D.R. and Shervais, J.W., 2015. Seismic imaging through the volcanic rocks of the Snake River Pla
	Insights from Project Hotspot. Geophysical Prospecting, 63(4-Hard Rock Seismic imaging), pp.919-936.
	Malehmir, A., Durrheim, R., Bellefleur, G., Urosevic, M., Juhlin, C., White, D.J., Milkereit, B. and Campbell, G., 20
	Seismic methods in mineral exploration and mine planning: A general overview of past and present case histories and a lo
740	into the future. Geophysics, 77(5), pp. WC173-WC190.
	Malehmir, A., Manzi, M., Draganov, D., Weckmann, U. and Auken, E., 2020. Introduction to the special issue on "Co
	effective and innovative mineral exploration solutions". Geophysical prospecting, 68(1), pp.:
	Manzi, M., Malehmir, A. and Durrheim, R., 2019. Giving the legacy seismic data the attention they deserve. First Break, 37
	<del>pp.89-96.</del>
745	McBride, J., Nelson, S.T., Mwakanyamale, K.E., Wolfe, E.E., Tingey, D.G. and Rey, K.A., 2021. Geophysical characterizat
	of volcanic layering. Journal of Applied Geophysics, 195, p.104494.
	McCormack, T., O'Connell, Y., Daly, E., Gill, L.W., Henry, T. and Perriquet, M., 2017. Characterisation of karst hydrogeok
	in Western Ireland using geophysical and hydraulic modelling techniques. Journal of Hydrology: Regional Studies, 10, pp
	<del>17 </del>
750	Meere, P.A., 1995. The structural evolution of the western Irish Variscides: an example of obsta
	tectonics? Tectonophysics, 246(1-3), pp.97-112.
	O'Connell, Y., Daly, E., Henry, T. and Brown, C., 2018. Terrestrial and marine electrical resistivity to identify groundway
	pathways in coastal karst aquifers. Near Surface Geophysics, 16(2), pp.164-175.
	Paige, C.C. and Saunders, M.A., 1982. LSQR: An algorithm for sparse linear equations and sparse least squares. As
755	Transactions on Mathematical Software (TOMS), 8(1), pp.43-71.
	Planke, S., Alvestad, E. and Eldholm, O., 1999. Seismic characteristics of basaltic extrusive and intrusive rocks. The Lead
	Edga 18(2) pp 242 248

and Carriedo, J., 2021. Reflection seismic imaging to unravel subsurface geological structures of the Zinkgruvan mining area,

	Pujol, J., Fuller, B.N. and Smithson, S.B., 1989. Interpretation of a vertical seismic profile conducted in the Columbia Plateau
	basalts. Geophysics, 54(10), pp.1258-1266.
	Sevastopulo, G.D. and Wyse Jackson, P.N., 2009. Carboniferous: Mississippian (Tournaisian and Viséan). The geology of
	<i>Ireland</i> , pp.215-268.
765	Singh, B. and Malinowski, M., 2023. Seismic imaging of mineral exploration targets: Evaluation of ray-vs. wave-equation-
	based pre-stack depth migrations for crooked 2d profiles. Minerals, 13(2), p.264.
	Sleeman, A.G., Pracht, M. and Claringbold, K., 1999. Geology of the Shannon Estuary: A geological description of the
	Shannon Estuary region including parts of Clare, Limerick and Kerry to accompany the bedrock geology 1: 100,000 Scale
	Map Series, Sheet 17, Shannon Estuary. Geological Survey of Ireland.
770	Slezak, P., Hitzman, M.W., van Acken, D., Dunlevy, E., Chew, D., Drakou, F. and Holdstock, M., 2023. Petrogenesis of the
	Limerick Igneous Suite: insights into the causes of post-eruptive alteration and the magmatic sources underlying the Iapetus
	Suture in SW Ireland. Journal of the Geological Society, 180(2), pp.jgs 2022-039.
	Slezak, P., Hnatyshin, D., Andrés, A., Dunlevy, E., Koch, H., Holdstock, M. and Hitzman, M.W., 2023. A review of the
	Limerick Igneous Suite: links to base-metal mineralization in the SW Irish Orefield. Irish Association of Economic Geology.
775	LAEG-50th Anniversary Volume.
	Somerville, I.D. and Jones, G.L., 1985. The Courceyan stratigraphy of the Pallaskenry Borehole, County Limerick,
	Ireland. Geological Journal, 20(4), pp.377-400.
	Somerville, I.D., Strogen, P. and Jones, G.L., 1992. Biostratigraphy of Dinantian limestones and associated volcanic rocks in
	the Limerick Syncline, Ireland. Geological Journal, 27(3), pp.201-22
780	Somerville, I.D., Waters, C.N. and Collinson, J.D., 2011. South Central Ireland.
	Strogen, P., 1983. The geology of the volcanic rocks of southeast County Limerick (Doctoral dissertation, University College
	<del>Dublin).</del>
	Strogen, P., 1988. The Carboniferous lithostratigraphy of southeast County Limerick, Ireland, and the origin of the Shannon
	Trough. Geological Journal, 23(2), pp.121-137.
785	Sullivan, E.C., Hardage, B.A., McGrail, B.P. and Davis, K.N., 2011. Breakthroughs in seismic and borehole characterization
	of basalt sequestration targets. Energy Procedia, 4, pp.5615-5622.
	Torremans, K., Kyne, R., Doyle, R., Güven, J.F. and Walsh, J.J., 2018. Controls on metal distributions at the Lisheen and
	Silvermines deposits: insights into fluid flow pathways in Irish-type Zn-Pb deposits. Economic Geology, 113(7), pp.1455-
	1477.—
790	Tryggvason, A., Rögnvaldsson, S.T. and Flóvenz, O.G., 2002. Three-dimensional imaging of the P-and S-wave velocity
	structure and earthquake locations beneath Southwest Iceland. Geophysical Journal International, 151(3), pp.848-866.
	Tryggvason, A. and Bergman, B., 2006. A traveltime reciprocity discrepancy in the Podvin & Lecomte time3d finite difference
	algorithm. Geophysical Journal International, 165(2), pp.432-435.
	Tyler, P.A., 1997. The geology and exploration potential of the Pallas Green project. Unpublished internal report by McKillen,
795	Tyler and Associates for Minco Ireland Limited.
	Vidal, O., Goffé, B. and Arndt, N., 2013. Metals for a low-carbon society. Nature Geoscience, 6(11), pp.894-896.
	Wilkinson, J.J., Hitzman, M.W., Archibald, S.M. and Piercey, S.J., 2015. The Irish Zn-Pb orefield: the view from
	2014. Current Perspectives on Zinc Deposits. Irish Association for Economic Geology, Dublin, pp.59-72.
	Ziolkowski, A., Hanssen, P., Gatliff, R., Jakubowicz, H., Dobson, A., Hampson, G., Li, X.Y. and Liu, E., 2003. Use of low
800	frequencies for sub-basalt imaging. Geophysical Prospecting, 51(3), pp.169-182.

migration. In First International Meeting for Applied Geoscience & Energy (pp. 2684-2688). Society of Exploration

760

Geophysicists.

- Alcalde, J., Carbonell, R., Pospiech, S., Gil, A., Bullock, L. A., and Tornos, F.: Preface: State of the art in mineral exploration, Solid Earth, 13, 1161–1168, https://doi.org/10.5194/se-13-1161-2022, 2022.
- Ali, S. H., Giurco, D., Arndt, N., Nickless, E., Brown, G., Demetriades, A., Durrheim, R., Enriquez, M. A., Kinnaird, J., Littleboy, A., Meinert, L. D., Oberhänsli, R., Salem, J., Schodde, R., Schneider, G., Vidal, O., and Yakovleva, N.: Mineral supply for sustainable development requires resource governance, Nature, 543, 367–372, https://doi.org/10.1038/nature21359, 2017.

**\$**10

815

820

325

- Ashton, J. H., Beach, A., Blakeman, R. J., Coller, D., Henry, P., Lee, R., Hitzman, M., Hope, C., Huleatt-James, S., O'Donovan, B., and Philcox, M. E.: Discovery of the Tara Deep Zn-Pb Mineralization at the Boliden Tara Mine, Navan, Ireland: Success with Modern Seismic Surveys., in: Metals, Minerals, and Society, vol. 21, edited by: Arribas R., A. M. and Mauk, J. L., Society of Economic Geologists, 0, https://doi.org/10.5382/SP.21.16, 2018.
- Bell, T., Turner, G., Bhat, G., and Knell, B.: Multiscale insights into the Mount Weld REE deposit from 2D and 3D active seismic survey data, in: Third International Meeting for Applied Geoscience & Energy Expanded Abstracts, Society of Exploration Geophysicists and American Association of Petroleum Geologists, 1653–1657, https://doi.org/10.1190/image2023-3912490.1, 2023.
- Benz, H. M., Chouet, B. A., Dawson, P. B., Lahr, J. C., Page, R. A., and Hole, J. A.: Three-dimensional P and S wave velocity structure of Redoubt Volcano, Alaska, Journal of Geophysical Research: Solid Earth, 101, 8111–8128, https://doi.org/10.1029/95JB03046, 1996.
- Blaney, D. and Coffey, E.: The volcano-stratigraphic setting of the Pallas Green Zn-Pb deposit, County Limerick. In: Andrew, C.J., Hitzman, M.W. & Stanley, G. Irish-type Deposits around the world, Irish Association for Economic Geology, Dublin, pp. 285-308. DOI: https://doi.org/10.61153/QHKU2937, 2023.
- Blaney, D. and Redmond, P. B.: Zinc-lead deposits of the Limerick Basin, Ireland, Current Perspectives on Zinc Deposits, 73–84, 2015.
- Bonini, M., Sani, F., and Antonielli, B.: Basin inversion and contractional reactivation of inherited normal faults: A review based on previous and new experimental models, Tectonophysics, 522–523, 55–88, https://doi.org/10.1016/j.tecto.2011.11.014, 2012.
- Chakraborti, P., Susin, V., Cavalcanti, G., and Melo, A.: Chargeability, Compressional Velocity (Vp), Density, Galvanic Electric Resistivity, Inductive Electric Conductivity, Magnetic Susceptibility, Portable X-Ray Fluorescence (pXRF), and Shear Velocity (Vs) of the Drillhole TC-2531-001 in Limerick Basin, Ireland., Zenodo, https://doi.org/10.5281/zenodo.16905925, 2025.
- Cheraghi, S., Hloušek, F., Buske, S., Malehmir, A., Adetunji, A., Haugaard, R., Snyder, D., and Vayavur, R.: Reflection seismic imaging across a greenstone belt, Abitibi (Ontario), Canada, Geophysical Prospecting, 71, 1096–1115, https://doi.org/10.1111/1365-2478.13284, 2023.
- Chew, D. M., Stillman, C. J., Holland, C. H., and Sanders, I. S.: Late Caledonian orogeny and magmatism, The geology of Ireland, 2, 143–173, 2009.
- Devuyst, F.-X. and Lees, A.: The initiation of Waulsortian buildups in Western Ireland, Sedimentology, 48, 1121–1148, https://doi.org/10.1046/j.1365-3091.2001.00411.x, 2001.

- Eaton, D. W., Milkereit, B., and Salisbury, M.: Seismic methods for deep mineral exploration: Mature technologies adapted to new targets, The Leading Edge, 22, 580–585, https://doi.org/10.1190/1.1587683, 2003.
- Eaton, D. W., Adam, E., Milkereit, B., Salisbury, M., Roberts, B., White, D., and Wright, J.: Enhancing base-metal exploration with seismic imaging This article is one of a series of papers published in this Special Issue on the theme Lithoprobe—parameters, processes, and the evolution of a continent., Canadian Journal of Earth Sciences, 47, 741–760, https://doi.org/10.1139/E09-047, 2010.

845

355

860

- Eberli, G. P., Baechle, G. T., Anselmetti, F. S., and Incze, M. L.: Factors controlling elastic properties in carbonate sediments and rocks, The Leading Edge, 22, 654–660, https://doi.org/10.1190/1.1599691, 2003.
- Elliott, H. A. L., Gernon, T. M., Roberts, S., and Hewson, C.: Basaltic maar-diatreme volcanism in the Lower Carboniferous of the Limerick Basin (SW Ireland), Bull Volcanol, 77, 37, https://doi.org/10.1007/s00445-015-0922-2, 2015.
- Fusciardi, L. P., Guven, J. F., Stewart, D. R. A., Carboni, V., Walsh, J. J., Kelly, J. G., Andrew, C. J., Ashton, J. H., Boland, M. B., and Earls, G.: The geology and genesis of the Lisheen Zn-Pb deposit, Co. Tipperary, Ireland, Europe's major base metal deposits, 455–481, 2003.
- 600 Geological Survey Ireland: Bedrock geology of Ireland map 1:100,000: Limerick Basin, Geological Survey Ireland, 2022.
  - Gil, A., Malehmir, A., Buske, S., Alcalde, J., Ayarza, P., Martínez, Y., Lindskog, L., Spicer, B., Carbonell, R., Orlowsky, D., Carriedo, J., and Hagerud, A.: Reflection seismic imaging to unravel subsurface geological structures of the Zinkgruvan mining area, central Sweden, Ore Geology Reviews, 137, 104306, https://doi.org/10.1016/j.oregeorev.2021.104306, 2021.
  - Gordon, P., Kelly, J. G. and van Lente, B.: NI 43-101 Independent Report on the Zinc-Lead Exploration Project at Stonepark, County Limerick, Ireland. www.groupelevenresources.com/Projects/Stonepark,2018.
  - Guven, J., Torremans, K., Johnson, S., and Hitzman, M.: The Rathdowney Trend, Ireland: Geological evolution and controls on Zn-Pb mineralization, Irish-Type Deposits around the World; Andrew, CJ, Hitzman, MW, Stanley, G., Eds, 329–362, 2023.
  - Hitzman, M. W.: Extensional faults that localize Irish syndiagenetic Zn-Pb Deposits and their reactivation during Variscan compression, SP, 155, 233–245, https://doi.org/10.1144/GSL.SP.1999.155.01.17, 1999.
  - Hool, A., Helbig, C., and Wierink, G.: Challenges and opportunities of the European Critical Raw Materials Act, Mineral Economics, 37, 661–668, https://doi.org/10.1007/s13563-023-00394-y, 2023.
  - Johnston, J. D.: Regional fluid flow and the genesis of Irish Carboniferous base metal deposits, Mineral. Deposita, 34, 571–598, https://doi.org/10.1007/s001260050221, 1999.
  - Johnston, J. D., Coller, D., Millar, G., and Critchley, M. F.: Basement structural controls on Carboniferous-hosted base metal mineral deposits in Ireland, Geological Society, London, Special Publications, 107, 1–21, <a href="https://doi.org/10.1144/GSL.SP.1996.107.01.02">https://doi.org/10.1144/GSL.SP.1996.107.01.02</a>, 1996.
  - Kyne, R., Torremans, K., Güven, J., Doyle, R., and Walsh, J.: 3-D Modeling of the Lisheen and Silvermines Deposits, County Tipperary, Ireland:Insights into Structural Controls on the Formation of Irish Zn-Pb Deposits, Economic Geology, 114, 93–116, https://doi.org/10.5382/econgeo.2019.4621, 2019.

- Lees, A.: The structure and origin of the Waulsortian (Lower Carboniferous) "reefs" of west-central Eire, Philosophical
  Transactions of the Royal Society of London. Series B, Biological Sciences, 247, 483–531,
  https://doi.org/10.1098/rstb.1964.0004, 1964.
  - Liberty, L. M., Schmitt, D. R., and Shervais, J. W.: Seismic imaging through the volcanic rocks of the Snake River Plain: insights from Project Hotspot, Geophysical Prospecting, 63, 919–936, https://doi.org/10.1111/1365-2478.12277, 2015.
- Malehmir, A., Durrheim, R., Bellefleur, G., Urosevic, M., Juhlin, C., White, D. J., Milkereit, B., and Campbell, G.: Seismic methods in mineral exploration and mine planning: A general overview of past and present case histories and a look into the future, GEOPHYSICS, 77, WC173–WC190, https://doi.org/10.1190/geo2012-0028.1, 2012.
  - Malehmir, A., Manzi, M., Draganov, D., Weckmann, U., and Auken, E. (Eds.): Special Issue: Cost-Effective and Innovative Mineral Exploration Solutions, Geophysical Prospecting, 68, 1–349, 2020.
  - Manzi, M., Malehmir, A., and Durrheim, R.: Giving the legacy seismic data the attention they deserve, First Break, 37, 89–96, https://doi.org/10.3997/1365-2397.n0050, 2019.

885

890

895

- McBride, J., Nelson, S. T., Mwakanyamale, K. E., Wolfe, E. E., Tingey, D. G., and Rey, K. A.: Geophysical characterization of volcanic layering, Journal of Applied Geophysics, 195, 104494, https://doi.org/10.1016/j.jappgeo.2021.104494, 2021.
- McCormack, T., O'Connell, Y., Daly, E., Gill, L. W., Henry, T., and Perriquet, M.: Characterisation of karst hydrogeology in Western Ireland using geophysical and hydraulic modelling techniques, Journal of Hydrology: Regional Studies, 10, 1–17, https://doi.org/10.1016/j.ejrh.2016.12.083, 2017.
- Meere, P. A.: The structural evolution of the western Irish Variscides: an example of obstacle tectonics?, Tectonophysics, 246, 97–112, https://doi.org/10.1016/0040-1951(94)00267-D, 1995.
- Melo, A., Chakraborti, P., Susin, V., Farrell, C., and Byrne, E.: Chargeability, Compressional Velocity (Vp), Density, Galvanic Electric Resistivity, Gamma Ray Spectrometry (K, Th, U), Inductive Electric Conductivity, Magnetic Susceptibility, Portable X-Ray Fluorescence (pXRF), and Shear Velocity (Vs) of the Drillhole G11-2531-01 in Limerick Basin, Ireland., Zenodo, https://doi.org/10.5281/zenodo.16905640, 2025a.
- Melo, A., Susin, V., Chakraborti, P., and Wei, N.: Methodology for measuring Chargeability, Compressional Velocity (Vp), Density, Galvanic Electric Resistivity, Gamma Ray Spectrometry (K, Th, U), Inductive Electric Conductivity, Magnetic Susceptibility, Portable X-Ray Fluorescence (XRF), and Shear Velocity (Vs) of drill core rock samples at the UCD Petrophysics Laboratory, Zenodo, https://doi.org/10.5281/zenodo.16903342, 2025b.
- de Morton, S. N., Wallace, M. W., Reed, C. P., Hewson, C., Redmond, P., Cross, E., and Moynihan, C.: The significance of Tournaisian tectonism in the Dublin basin: Implications for basin evolution and zinc-lead mineralization in the Irish Midlands, Sedimentary Geology, 330, 32–46, https://doi.org/10.1016/j.sedgeo.2015.09.017, 2015.
- O'Connell, Y., Daly, E., Henry, T., and Brown, C.: Terrestrial and marine electrical resistivity to identify groundwater pathways in coastal karst aquifers, Near Surface Geophysics, 16, 164–175, https://doi.org/10.3997/1873-0604.2017062, 2018.
- Paige, C. C. and Saunders, M. A.: LSQR: An Algorithm for Sparse Linear Equations and Sparse Least Squares, ACM Trans. Math. Softw., 8, 43–71, https://doi.org/10.1145/355984.355989, 1982.
- Planke, S., Alvestad, E., and Eldholm, O.: Seismic characteristics of basaltic extrusive and intrusive rocks, The Leading Edge, 18, 342–348, https://doi.org/10.1190/1.1438289, 1999.

Pu, Y., Liu, G., Wang, D., Huang, H., and Wang, P.: Wave-equation traveltime and amplitude for Kirchhoff migration, in: First International Meeting for Applied Geoscience & Energy Expanded Abstracts, Society of Exploration Geophysicists, 2684–2688, https://doi.org/10.1190/segam2021-3583642.1, 2021.

Pujol, J., Fuller, B. N., and Smithson, S. B.: Interpretation of a vertical seismic profile conducted in the Columbia Plateau basalts, GEOPHYSICS, 54, 1258–1266, https://doi.org/10.1190/1.1442585, 1989.

Robertson Geo: Mining & Minerals, 002 RGO/18, https://www.robertson-geo.com, 2019.

910

915

920

925

930

935

Salisbury, M. H., Bernd, M., Ascough, G., Adair, R., Matthews, L., Schmitt, D. R., Mwenifumbo, J., Eaton, D. W., and Wu, J.: Physical properties and seismic imaging of massive sulfides, Geophysics, 65, 1882–1889, https://doi.org/10.1190/1.1444872, 2000.

Sevastopulo, G. D. and Wyse Jackson, P. N.: Carboniferous: Mississippian (Tournaisian and Viséan), The geology of Ireland, 215–268, 2009.

Singh, B. and Malinowski, M.: Seismic Imaging of Mineral Exploration Targets: Evaluation of Ray- vs. Wave-Equation-Based Pre-Stack Depth Migrations for Crooked 2D Profiles, Minerals, 13, 264, https://doi.org/10.3390/min13020264, 2023.

Slezak, P., Hitzman, M. W., van Acken, D., Dunlevy, E., Chew, D., Drakou, F., and Holdstock, M.: Petrogenesis of the Limerick Igneous Suite: insights into the causes of post-eruptive alteration and the magmatic sources underlying the Iapetus Suture in SW Ireland, Journal of the Geological Society, 180, jgs2022-039, https://doi.org/10.1144/jgs2022-039, 2023.

Somerville, I. D. and Jones, G. L. I.: The Courceyan stratigraphy of the Pallaskenry Borehole, County Limerick, Ireland, Geological Journal, 20, 377–400, https://doi.org/10.1002/gj.3350200406, 1985.

Somerville, I. D., Strogen, P., and Jones, G. Li.: Biostratigraphy of Dinantian limestones and associated volcanic rocks in the Limerick Syncline, Ireland, Geological Journal, 27, 201–220, https://doi.org/10.1002/gj.3350270302, 1992.

Somerville, I. D., Waters, C. N., and Collinson, J. D.: South Central Ireland, https://doi.org/10.1144/SR26.22, 2011.

Strogen, P.: The geology of the volcanic rocks of southeast County Limerick, PhD Thesis, University College Dublin, 1983.

Strogen, P.: The carboniferous lithostratigraphy of Southeast County Limerick, Ireland, and the origin of the shannon trough, Geological Journal, 23, 121–137, https://doi.org/10.1002/gj.3350230202, 1988.

Sullivan, E. C., Hardage, B. A., McGrail, B. P., and Davis, K. N.: Breakthroughs in seismic and borehole characterization of Basalt sequestration targets, Energy Procedia, 4, 5615–5622, https://doi.org/10.1016/j.egypro.2011.02.551, 2011.

Susin, V., Melo, A., Chakraborti, P., Farrell, C., and Byrne, E.: Chargeability, Compressional Velocity (Vp), Density, Galvanic Electric Resistivity, Gamma Ray Spectrometry (K, Th, U), Inductive Electric Conductivity, Magnetic Susceptibility, Portable X-Ray Fluorescence (pXRF), and Shear Velocity (Vs) of the Drillhole G11-2638-06 in Limerick Basin, Ireland., Zenodo, https://doi.org/10.5281/zenodo.16905792, 2025a.

Susin, V., Chakraborti, P., Melo, A., and Cavalcanti, G.: Chargeability, Compressional Velocity (Vp), Density, Galvanic Electric Resistivity, Gamma Ray Spectrometry (K, Th, U), Inductive Electric Conductivity, Magnetic Susceptibility, Portable X-Ray Fluorescence (pXRF), and Shear Velocity (Vs) of the Drillhole TC-2638-004 in Limerick Basin, Ireland., Zenodo, <a href="https://doi.org/10.5281/zenodo.17098955">https://doi.org/10.5281/zenodo.17098955</a>, 2025b.

- Susin, V., Chakraborti, P., Melo, A., and Cavalcanti, G.: Chargeability, Compressional Velocity (Vp), Density, Galvanic Electric Resistivity, Gamma Ray Spectrometry (K, Th, U), Inductive Electric Conductivity, Magnetic Susceptibility, Portable X-Ray Fluorescence (pXRF), and Shear Velocity (Vs) of the Drillhole TC-2638-008 in Limerick Basin, Ireland., Zenodo, https://doi.org/10.5281/zenodo.17099141, 2025c.
  - Susin, V., Chakraborti, P., Melo, A., and Cavalcanti, G.: Chargeability, Compressional Velocity (Vp), Density, Galvanic Electric Resistivity, Gamma Ray Spectrometry (K, Th, U), Inductive Electric Conductivity, Magnetic Susceptibility, Portable X-Ray Fluorescence (pXRF), and Shear Velocity (Vs) of the Drillhole TC-2638-026 in Limerick Basin, Ireland., Zenodo, https://doi.org/10.5281/zenodo.17099214, 2025d.

950

955

960

965

970

- Susin, V., Chakraborti, P., Melo, A., and Cavalcanti, G.: Chargeability, Compressional Velocity (Vp), Density, Galvanic Electric Resistivity, Gamma Ray Spectrometry (K, Th, U), Inductive Electric Conductivity, Magnetic Susceptibility, Portable X-Ray Fluorescence (pXRF), and Shear Velocity (Vs) of the Drillhole TC-2638-036 in Limerick Basin, Ireland., Zenodo, https://doi.org/10.5281/zenodo.17099312, 2025e.
- Susin, V., Chakraborti, P., Melo, A., and Cavalcanti, G.: Chargeability, Compressional Velocity (Vp), Density, Galvanic Electric Resistivity, Gamma Ray Spectrometry (K, Th, U), Inductive Electric Conductivity, Magnetic Susceptibility, Portable X-Ray Fluorescence (pXRF), and Shear Velocity (Vs) of the Drillhole TC-2638-074 in Limerick Basin, Ireland., Zenodo, https://doi.org/10.5281/zenodo.17099380, 2025f.
- Susin, V., Chakraborti, P., Melo, A., and Cavalcanti, G.: Chargeability, Compressional Velocity (Vp), Density, Galvanic Electric Resistivity, Gamma Ray Spectrometry (K, Th, U), Inductive Electric Conductivity, Magnetic Susceptibility, Portable X-Ray Fluorescence (pXRF), and Shear Velocity (Vs) of the Drillhole TC-2638-088 in Limerick Basin, Ireland., Zenodo, https://doi.org/10.5281/zenodo.17099469, 2025g.
- Susin, V., Chakraborti, P., Melo, A., and Cavalcanti, G.: Chargeability, Compressional Velocity (Vp), Density, Galvanic Electric Resistivity, Gamma Ray Spectrometry (K, Th, U), Inductive Electric Conductivity, Magnetic Susceptibility, Portable X-Ray Fluorescence (pXRF), and Shear Velocity (Vs) of the Drillhole TC-2638-101 in Limerick Basin, Ireland., Zenodo, https://doi.org/10.5281/zenodo.17099518, 2025h.
- Torremans, K., Kyne, R., Doyle, R., Güven, J. F., and Walsh, J. J.: Controls on Metal Distributions at the Lisheen and Silvermines Deposits: Insights into Fluid Flow Pathways in Irish-Type Zn-Pb Deposits, Economic Geology, 113, 1455–1477, https://doi.org/10.5382/econgeo.2018.4598, 2018.
- Tryggvason, A. and Bergman, B.: A traveltime reciprocity discrepancy in the Podvin & Lecomte time3d finite difference algorithm, Geophys J Int, 165, 432–435, https://doi.org/10.1111/j.1365-246X.2006.02925.x, 2006.
- Tryggvason, A., Rögnvaldsson, S. Th., and Flóvenz, Ó. G.: Three-dimensional imaging of the P- and S-wave velocity structure and earthquake locations beneath Southwest Iceland, Geophys J Int, 151, 848–866, https://doi.org/10.1046/j.1365-246X.2002.01812.x, 2002.
- Tyler, P. A.: The geology and exploration potential of the Pallas Green project, Unpublished internal report by McKillen, Tyler and Associates for Minco Ireland Limited, 1997.
- Vidal, O., Goffé, B., and Arndt, N.: Metals for a low-carbon society, Nature Geosci, 6, 894–896, https://doi.org/10.1038/ngeo1993, 2013.

Walsh, J. J., Torremans, K., Güven, J., Kyne, R., Conneally, J., and Bonson, C.: Fault-Controlled Fluid Flow Within Extensional Basins and Its Implications for Sedimentary Rock-Hosted Mineral Deposits, in: Metals, Minerals, and Society, vol. 21, edited by: Arribas R., A. M. and Mauk, J. L., Society of Economic Geologists, 0, https://doi.org/10.5382/SP.21.11, 2018.

Wilkinson, J. J.: Tracing metals from source to sink in Irish-type Zn–Pb (-Ba-Ag) deposits, Irish-type Zn–Pb deposits around the world, Editors: Andrew, CJ, Hitzman, MW, and Stanley, G, 147–168, 2023.

980

985

Wilkinson, J. J., Crowther, H. L., and Coles, B. J.: Chemical mass transfer during hydrothermal alteration of carbonates: Controls of seafloor subsidence, sedimentation and Zn–Pb mineralization in the Irish Carboniferous, Chemical Geology, 289, 55–75, https://doi.org/10.1016/j.chemgeo.2011.07.008, 2011.

Wilkinson, J.J., Hitzman, M.W., Archibald, S.M. and Piercey, S.J.: The Irish Zn-Pb orefield: the view from 2014. Current Perspectives on Zinc Deposits. Irish Association for Economic Geology, Dublin, pp.59-72, 2015.

Ziolkowski, A., Hanssen, P., Gatliff, R., Jakubowicz, H., Dobson, A., Hampson, G., Li, X.-Y., and Liu, E.: Use of low frequencies for sub-basalt imaging, Geophysical Prospecting, 51, 169–182, https://doi.org/10.1046/j.1365-2478.2003.00363.x, 2003.

Formatted: Font: 10 pt

Formatted: Bibliography, Line spacing: 1.5 lines